Available online at www.sciencedirect.com
ScienceDirect
Geochimica et Cosmochimica Acta 75 (2011) 3318–3334
Geochimica et Cosmochimica Acta
www.elsevier.com/locate/gca

Iron and magnesium isotopic compositions of peridotite xenoliths from Eastern China

Fang Huang [a,b,c,*], Zhaofeng Zhang [b], Craig C. Lundstrom [b], Xiachen Zhi [c]

[a] Institute of Geochemistry and Petrology, ETH Zurich, CH-8092 Zurich, Switzerland
[b] Department of Geology, University of Illinois at Urbana-Champaign, 245 NHB, 1301 W. Green Street, Urbana, IL 61801, USA
[c] CAS Key Laboratory of Crust–Mantle Materials and Environments, School of Earth and Space Sciences, University of Science and Technology of China, Hefei 230026, China

Received 29 June 2010; accepted in revised form 15 February 2011; available online 30 March 2011

Abstract

We present high-precision measurements of Mg and Fe isotopic compositions of olivine, orthopyroxene (opx), and clinopyroxene (cpx) for 18 lherzolite xenoliths from east central China and provide the first combined Fe and Mg isotopic study of the upper mantle. δ^{56}Fe in olivines varies from 0.18‰ to −0.22‰ with an average of −0.01 ± 0.18‰ (2SD, $n = 18$), opx from 0.24‰ to −0.22‰ with an average of 0.04 ± 0.20‰, and cpx from 0.24‰ to −0.16‰ with an average of 0.10 ± 0.19‰. δ^{26}Mg of olivines varies from −0.25‰ to −0.42‰ with an average of −0.34 ± 0.10‰ (2SD, $n = 18$), opx from −0.19‰ to −0.34‰ with an average of −0.25 ± 0.10‰, and cpx from −0.09‰ to −0.43‰ with an average of −0.24 ± 0.18‰. Although current precision (~±0.06‰ for δ^{56}Fe; ±0.10‰ for δ^{26}Mg, 2SD) limits the ability to analytically distinguish inter-mineral isotopic fractionations, systematic behavior of inter-mineral fractionation for both Fe and Mg is statistically observed: $\Delta^{56}Fe_{ol-cpx} = -0.10 \pm 0.12‰$ (2SD, $n = 18$); $\Delta^{56}Fe_{ol-opx} = -0.05 \pm 0.11‰$; $\Delta^{26}Mg_{ol-opx} = -0.09 \pm 0.12‰$; $\Delta^{26}Mg_{ol-cpx} = -0.10 \pm 0.15‰$. Fe and Mg isotopic composition of bulk rocks were calculated based on the modes of olivine, opx, and cpx. The average δ^{56}Fe of peridotites in this study is 0.01 ± 0.17‰ (2SD, $n = 18$), similar to the values of chondrites but slightly lower than mid-ocean ridge basalts (MORB) and oceanic island basalts (OIB). The average δ^{26}Mg is −0.30 ± 0.09‰, indistinguishable from chondrites, MORB, and OIB. Our data support the conclusion that the bulk silicate Earth (BSE) has chondritic δ^{56}Fe and δ^{26}Mg.

The origin of inter-mineral fractionations of Fe and Mg isotopic ratios remains debated. δ^{56}Fe between the main peridotite minerals shows positive linear correlations with slopes within error of unity, strongly suggesting intra-sample mineral–mineral Fe and Mg isotopic equilibrium. Because inter-mineral isotopic equilibrium should be reached earlier than major element equilibrium via chemical diffusion at mantle temperatures, Fe and Mg isotope ratios of coexisting minerals could be useful tools for justifying mineral thermometry and barometry on the basis of chemical equilibrium between minerals. Although most peridotites in this study exhibit a narrow range in δ^{56}Fe, the larger deviations from average δ^{56}Fe for three samples likely indicate changes due to metasomatic processes. Two samples show heavy δ^{56}Fe relative to the average and they also have high La/Yb and total Fe content, consistent with metasomatic reaction between peridotite and Fe-rich and isotopically heavy melt. The other sample has light δ^{56}Fe and slightly heavy δ^{26}Mg, which may reflect Fe–Mg inter-diffusion between peridotite and percolating melt.

© 2011 Elsevier Ltd. All rights reserved.

1. INTRODUCTION

Iron and magnesium are two of the major constituent elements of the mantle, being primary metal cations in the most common upper mantle minerals such as olivine, orthopyroxene (opx), clinopyroxene (cpx), garnet, and

* Corresponding author at: CAS Key Laboratory of Crust–Mantle Materials and Environments, School of Earth and Space Sciences, University of Science and Technology of China, Hefei 230026, China.
E-mail addresses: fhuang@ustc.edu.cn, huangfang426@hotmail.com (F. Huang).

0016-7037/$ - see front matter © 2011 Elsevier Ltd. All rights reserved.
doi:10.1016/j.gca.2011.03.036

spinel. Iron has two common valences (2+ and 3+) in mantle minerals and melts, with Fe^{3+} being more incompatible than Fe^{2+} during partial melting. Several recent studies have revealed small but analytically significant variation in the Fe isotopic composition of mantle rocks and minerals (Zhu et al., 2002; Beard and Johnson, 2004; Williams et al., 2004, 2005; Weyer et al., 2005, 2007; Weyer and Ionov, 2007; Zhao et al., 2010). Because light Fe isotopes should preferentially partition into Fe^{2+} sites in minerals, melting of the upper mantle has been suggested to produce melts enriched with heavy Fe isotopes, leaving an isotopically lighter residue behind (Weyer and Ionov, 2007; Dauphas et al., 2009a). In addition, metasomatism and kinetic processes (chemical or thermal diffusion) also have the potential to cause Fe isotope fractionation in mantle peridotites (Weyer and Ionov, 2007; Huang et al., 2009a, 2010a; Richter et al., 2008, 2009; Zhao et al., 2010). Therefore Fe isotopes provide a new tracer for studying the evolution of a heterogeneous upper mantle.

The mantle is the Earth's largest reservoir of Mg. While Mg isotope data for igneous rocks and mantle minerals have been increasingly reported in the last few years (Pearson et al., 2006; Teng et al., 2007, 2010a; Wiechert and Halliday, 2007; Handler et al., 2009; Huang et al., 2009b; Yang et al., 2009; Young et al., 2009; Bourdon et al., 2010; Chakrabarti and Jacobsen, 2010; Li et al., 2010; Liu et al., 2010), the magnesium isotopic composition of the bulk silicate Earth (BSE) remains poorly constrained and application of Mg isotopes to studying mantle geochemistry is still at an early stage. There remain debates about the average Mg isotopic composition of the upper mantle and whether the BSE has a chondritic or non-chondritic Mg isotopic composition (Wiechert and Halliday, 2007; Handler et al., 2009; Yang et al., 2009; Young et al., 2009; Chakrabarti and Jacobsen, 2010; Teng et al., 2010a). Knowledge of the Mg isotopic variation in the upper mantle is critical to understanding the cycling of Mg during magmatism, chemical weathering, diagenesis, and crustal recycling. Finally, because high precision Mg isotopic data for mantle minerals are still few in number, it is unclear whether there is inter-mineral Mg isotope fractionation in mantle peridotites. For instance, Yang et al. (2009) suggest identical Mg isotopic compositions of mantle minerals within an external precision of ±0.1‰ (2SD), while other studies (Handler et al., 2009; Young et al., 2009; Chakrabarti and Jacobsen, 2010) arguably show pyroxenes to be slightly heavier in Mg isotopic composition than coexisting olivines.

The geochemical behaviors of Mg and Fe are intrinsically linked by their inter substitution within solid solution minerals in the mantle. A primary difference between their isotopic behavior is that Mg isotope ratios should not be fractionated by the partitioning of different valence states between phases like Fe. Therefore, combined analyses of the Fe and Mg isotope systems could provide new insight towards sorting out the behavior of these elements in the mantle. Indeed, a recent experimental study shows the complex inter-diffusion behavior within olivine during diffusive reaction with melt (Lundstrom et al., 2011). Here we present the first combined Fe and Mg isotopic study of mantle minerals from a set of well-characterized peridotite xenoliths from the Subei Basin in the Yangtze Craton, China. These peridotites experienced significant melt extraction at ~1.8 Ga and extensive melt percolation during Cenozoic magmatism (Reisberg et al., 2005). Thus, they provide a good opportunity to study Fe and Mg isotopic variations during upper mantle evolution. Our goals are to constrain the Fe and Mg isotopic composition of the upper mantle relative to chondritic compositions in the literature. Additionally, we investigate inter-mineral isotopic fractionation at mantle temperatures. Our results show that while most peridotites in this study display a narrow range in $\delta^{56}Fe$ and $\delta^{26}Mg$, metasomatic processes and Fe–Mg inter-diffusion between peridotite and percolating melt likely play a role in fractionating Fe–Mg isotopes in the upper mantle.

2. GEOLOGIC BACKGROUND AND SAMPLE DESCRIPTION

Eastern China consists of the North China Craton (NCC) and the Yangtze Craton (YC) with the Qinling-Dabie-Sulu ultrahigh pressure metamorphic zone as the boundary between them (Fig. 1). The NCC is the largest craton in China and has an early Archean to Paleoproterozoic basement (e.g., Jahn et al., 1987). The YC is mainly Proterozoic, although Archean crust and old zircons have been increasingly observed in its northwestern part suggesting multi-stage reworking of this craton since the Archean (Zhang et al., 2006). Eastern China was marked by two important geologic events during the Phanerozoic: lithospheric thinning from the Ordovician to the Cenozoic and continental collision between the NCC and the YC in the Triassic. Observation of Ordovician diamond-bearing kimberlites and mantle xenoliths suggests that a thick (~200 km) cold lithosphere existed in the NCC in the Paleozoic (e.g., Griffin et al., 1998; Menzies and Xu, 1998), dramatically different from the current thin lithosphere indicated by seismologic studies (e.g., Chen et al., 2008, 2009b). This suggests that the lithosphere has been significantly thinned by ~100 km since the Paleozoic. Continental collision occurred along the Qinling-Dabie-Sulu zone in the Triassic (e.g., Li et al., 1993), forming the eastern part of the central orogenic belt in China. The Sulu belt was displaced northward ~500 km relative to the Dabie orogen by the Tanlu strike-slip fault in the early Cretaceous (Zhu et al., 2005).

Cenozoic basaltic volcanism occurred widely in eastern China, probably due to further extensional lithospheric thinning. These basalts mainly follow the major regional faults and bear abundant peridotite xenoliths (e.g., Reisberg et al., 2005; Chen et al., 2009a; Yang et al., 2009). Eighteen samples (LHLS1 to LHLS18) in this study were collected from Neogene alkali basalts in the Lianshan area in the Subei basin (Fig. 1) (see Fig. 1 in Reisberg et al. (2005) for more specific sample location). These xenoliths were well documented for whole rock major and trace elements and Re–Os isotopic compositions, which suggested a model age of about 1.8 Ga (Reisberg et al., 2005). Most samples (except LHLS12) are fresh coarse-grained spinel-facies peridotites, while LHLS12 is slightly serpentinized. The xenoliths have protogranular or protogranular/porphyroclastic

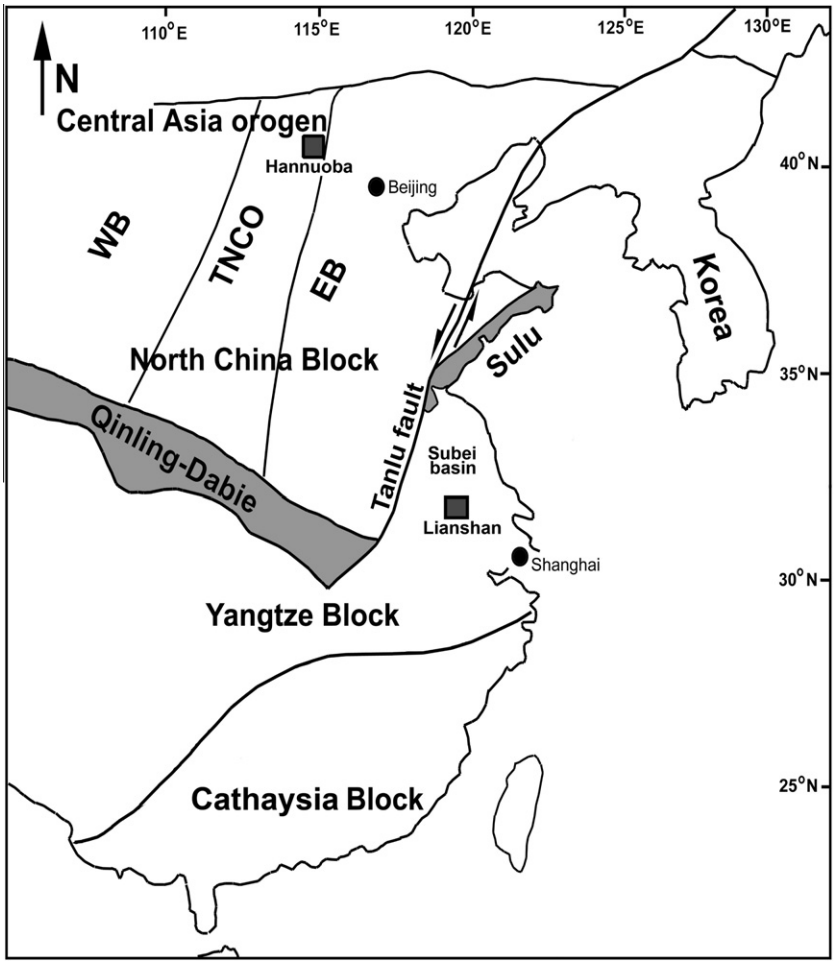

Fig. 1. A simplified geological map for Eastern China with sample location. The North China Block consists of the Western block (WB) the Trans-North China orogen (TNCO), and the Eastern block (EB).

textures with sizes ranging from a few centimeters up to one meter. Most xenoliths do not have preferential mineral orientations except LHLS2 which has parallel elongated olivines. More sample description details can be found in Reisberg et al. (2005).

3. ANALYTICAL METHODS

Major element compositions of olivine, opx, and cpx were determined by electron microprobe analysis (JEOL, JXA-8200) at the Institute of Geochemistry and Petrology at the ETH Zurich and spinels by Cameca CAMEBAX at the Nicholas School of Environment and Earth Sciences of Duke University. Analytical conditions included an accelerating voltage of 15 kV, a beam current of 20 nA, and a beam size of 1–10 μm. A variety of silicates and oxides were used as standards. External errors were calculated based on 3–6 analyses of different spots. Data are available in Supplementary materials online S-Table 1.

Fe and Mg isotopic ratios were measured at the Department of Geology at the University of Illinois at Urbana-Champaign (UIUC). Fresh single mineral grains (~2–4 mg) were handpicked under binocular microscope and cleaned three times in an ultra-sonic bath for 10 min with ethanol. These were then digested in a 7 ml capped Teflon beaker with a mixture of concentrated HF and HNO_3 (3:1) on a hotplate for 2–4 days. After repeated evaporation using aqua regia and concentrated HNO_3 to remove residual fluorides and obtain full digestion, the samples were dissolved in 8 N HCl to provide a stock bulk solution ready for chromatographic separation of Fe.

Fe was purified using anion resin (Bio-Rad AG1-X8) conditioned with 8 N HCl. Matrix elements were removed by washing with 8 N HCl (washes were collected to assess the loss of Fe for yield check). Fe was eluted using 0.5 N HCl and H_2O followed by 8 N HNO_3 and H_2O. This procedure does not separate Zn from Fe. However, because the Zn content in the xenolith samples ranges from 47 to 63 ppm (Reisberg et al., 2005), the matrix effect of Zn on Fe isotope analysis is negligible. Mg purification followed the established procedure of Huang et al. (2009b). Approximately 0.5 ml aliquots of the stock bulk solution were dried down, evaporated with concentrated HNO_3, and then dissolved in 0.5 ml 1 N HNO_3 for chromatographic separation. Mg was separated in pre-cleaned Bio-Rad cation resin (AG50-X12) columns using 1 N HNO_3. Solutions

before and after the Mg cut were collected to check the recovery of Mg by comparing the amount of Mg in the different cuts. A pure Mg solution with high yield was obtained by two passes through the column for cpx and one pass for opx and olivine. Procedural blanks for Fe and Mg were measured by comparison with the signal intensity of standard solutions with known concentration; both were <10 ng, which are insignificant relative to the amount of Fe and Mg put through chemical purification (>20 μg). This procedure does not completely remove Ni from Mg. However, the Ni content is below the level that can cause significant matrix effects during Mg isotope analysis (Huang et al., 2009b).

Fe isotopic ratios were reported relative to IRMM-14 and Mg to DSM-3 in delta notation: $\delta^{56}Fe = 1000 \times [(^{56}Fe/^{54}Fe)_{sample}/(^{56}Fe/^{54}Fe)_{IRMM\text{-}14} - 1]$ (‰), and $\delta^{26}Mg = 1000 \times [(^{26}Mg/^{24}Mg)_{sample}/(^{26}Mg/^{24}Mg)_{DSM\text{-}3} - 1]$ (‰). IRMM-14 is a pure Fe metal reference material with a Fe isotopic composition about 0.1‰ lighter than that of the mean mafic Earth (Beard and Johnson, 2004). Fe and Mg isotopes were measured by standard bracketing methods using a Nu-Plasma MC-ICP-MS equipped with a Cetac ASX-110 automatic sampler and a DSN-100 Desolvating Nebulizer System. Before the isotopic measurement, the DSN was washed with 0.8 N HNO_3 twice followed by 0.3 N HNO_3 twice. Backgrounds were measured and subtracted using electrostatic analyzer (ESA) deflection. Prior to isotope analysis, yields and matrix elements were carefully checked to insure that the chemical procedure achieved high recovery rates (>99.5%) and excellent separation from matrix elements (e.g., signal intensity ratios of the total matrix relative to Fe or Mg always <5%). Iron solutions were diluted to 1.5 ppm for analysis and bracketed with IRMM-14 at the same concentration. ^{54}Fe, ^{56}Fe, and ^{57}Fe (along with ^{53}Cr for correcting any ^{54}Cr interference) were measured in static mode on L3, H4, and H6 Faraday cups, respectively. Contributions from isobaric interferences ($^{40}Ar^{14}N$ on ^{54}Fe and $^{40}Ar^{16}O$ on ^{56}Fe) were eliminated by measuring in pseudo-high resolution mode with M/ΔM of ~8000. The long-term (6 month) average $\delta^{56}Fe$ of 28 analyses of ETH hematite was 0.59 ± 0.05‰ (2SD), in agreement with the recommended value (Table 1) (Williams et al., 2004, 2005; Dideriksen et al., 2006). The average $\delta^{56}Fe$ of 55 analyses of our in-house standard (UIFe) was 0.71 ± 0.09‰. $\delta^{56}Fe$ of three USGS whole rock standards, BIR-1, AGV-1, and BCR-2, were 0.06 ± 0.03‰ ($n = 4$), 0.15 ± 0.03‰ ($n = 4$), and 0.09 ± 0.04‰ ($n = 4$) (Table 1), respectively, in good agreement with the literature values (e.g., Beard et al., 2003; Poitrasson et al., 2004; Williams et al., 2005; Dauphas and Rouxel, 2006; Dideriksen et al., 2006; Dauphas et al., 2009a,b; Wombacher et al., 2009; Craddock and Dauphas, 2011). Fe three-isotope plot of all mantle mineral samples defines a line with a slope of 1.497 ± 0.036 (Fig. 2), consistent with the theoretical kinetic and equilibrium fractionation values for Fe isotopes (1.487 and 1.474, respectively) (Young et al., 2002). The average external precision of $\delta^{56}Fe$ of mantle minerals is ~0.06‰ (2SD) (Table 2). Most duplicated analyses show excellent reproducibility at better than 0.04‰.

Mg isotope analyses were performed in low resolution (M/ΔM of ~400). ^{24}Mg, ^{25}Mg, and ^{26}Mg signals were measured in static mode on L5, axial, and H6 Faraday cups. Each measurement of a sample or standard represents 10 ratio determinations of 10 s integration time. Purified Mg solutions (~0.2 ppm) were repeatedly bracketed by DSM-3 for four times in a session, producing a ^{24}Mg signal of ~16 V at an uptake rate of 0.1 ml/min. The concentrations of the bracketing standards and samples were carefully adjusted to be within 5% of each other. Because our recent study showed that $\delta^{26}Mg$ of weak standard solutions consistently shifted to lighter values by ~0.2‰ during storage in fluorinated plastic (PTFE or Teflon®) bottles (Huang et al., 2009b), all running solutions of samples and standards were freshly diluted from concentrated bulk solutions (>5 ppm) to avoid errors possibly caused by solution storage. Three standard solutions (CAM-1, UIMg-1, and BCR-1) were regularly measured to monitor instrumental stability and reproducibility.

The accuracy and precision of Mg isotope analyses in the UIUC laboratory can be assessed by measurements of well-characterized standards and duplicated analyses of mineral samples. Huang et al. (2009b) reported high precision data for $\delta^{26}Mg$ of three mono-element solutions (DSM-3, CAM-1, and UIMg-1) and 11 whole rock standards (including peridotite, basalt, andesite, and granite). A detailed comparison of $\delta^{26}Mg$ in standards reported from different laboratories is given in Table 1 and discussed in Section 5.1. Overall, the long-term precision of $\delta^{26}Mg$ is about 0.11‰ (2SD) based on repeated analyses of the whole rock and in-house mono-element standards (Huang et al., 2009b). Repeated analyses (new digestion) of xenolith minerals indicate that the reproducibility of our Mg isotope data is ~0.10‰ (Table 3). Finally, a magnesium three-isotope plot of mineral samples in this study produces a line with a slope of 0.506 ± 0.020 (Fig. 2), in good agreement with the theoretical mass-dependent kinetic and equilibrium fractionation values (0.510 and 0.521, respectively) (Young et al., 2002).

4. RESULTS

Mineral element abundances are presented in the supplemental information (S-Table 1). The Mg# of olivines varies slightly from 88.9 to 91.3, consistent with the whole rock data in Reisberg et al. (2005). Mg# for cpx and opx ranges from 90.0 to 94.1 and from 89.3 to 91.6, respectively. Mineral modes calculated from bulk rock and mineral major element compositions using the least-squares method differ slightly from the values determined by point counting in thin sections, which may reflect a heterogeneous distribution of mineral modes at thin section scale. The calculated olivine modes vary from 52.5 to 73.5 wt.%, contributing 65–84% to the bulk Mg and 68–83% to the bulk Fe budget of a given peridotite sample. Modes of spinel vary from 0.1 to 2.3 wt.%, which only contributes <2.5% for Fe and <1% for Mg. Therefore, the effect of spinel on Fe and Mg isotopic compositions of the whole rock is minor.

Fe isotope compositions of olivines, opx, and cpx from 18 peridotite xenoliths are listed in Tables 2 and 4, respectively. Except for three outliers (LHLS5, 6, and 16), $\delta^{56}Fe$ of most minerals show narrow variations with olivines

Table 1
Comparison of δ^{26}Mg (‰) and δ^{56}Fe (‰) of standards measured in UIUC with literature data.

δ^{56}Fe	BIR-1	AGV-1	BCR-2	ETH hematite
Data measured in UIUC	0.06 ± 0.03	0.15 ± 0.03	0.09 ± 0.04	0.59 ± 0.05
Beard et al. (2003)		0.13 ± 0.10		
Poitrasson et al. (2004)*	0.07 ± 0.04	0.09 ± 0.05		0.53 ± 0.02
Weyer et al. (2005)	0.06 ± 0.04		0.08 ± 0.05	
Williams et al. (2005)*	0.06 ± 0.09			0.55 ± 0.09
Schoenberg and Blanckenburg (2006)	0.05 ± 0.05			
Dauphas et al. (2009b)			0.09 ± 0.03	
Dideriksen et al. (2006)	0.12 ± 0.06			0.58 ± 0.05
Wombacher et al. (2009)	0.03 ± 0.03		0.09 ± 0.06	
Heimann et al. (2008)		0.11 ± 0.05		

δ^{26}Mg	CAM-1	BCR-1	BCR-2	BHVO-1	BHVO-2	DTS-1	DTS-2	PCC-1	GA	GSN-1
Data measured in UIUC	−2.63 ± 0.11	−0.30 ± 0.11	−0.34 ± 0.12	−0.30 ± 0.08		−0.33 ± 0.14		−0.22 ± 0.10	−0.34 ± 0.15	−0.24 ± 0.23
Galy et al. (2003)	−2.58 ± 0.14									
Young and Galy (2004)		−0.37 ± 0.11								
Bizzarro et al. (2005)			−0.17 ± 0.35	−0.12 ± 0.15	−0.16 ± 0.10					
Wiecher and Halliday (2007)		−0.09 ± 0.27			−0.14 ± 0.23					
Teng et al. (2007)		−0.34 ± 0.06	−0.30 ± 0.08							
Tipper et al. (2008a)	−2.59 ± 0.09		−0.16 ± 0.11							
Pogge von Strandmann et al. (2008)	−2.78 ± 0.15				−0.25 ± 0.11					
Yang et al. (2009)	−2.63 ± 0.09					−0.30 ± 0.05	−0.38 ± 0.14 −0.32 ± 0.07			
Young et al. (2009)	−2.52, −2.72, −2.71									
Bolou-Bi et al. (2009)	−2.62 ± 0.13								−0.75 ± 0.14	
Wombacher et al. (2009)	−2.64 ± 0.23		−0.14 ± 0.11			−0.25 ± 0.08				
Chakrabarti and Jacobsen (2010)	−2.58 ± 0.16	−0.58 ± 0.29		−0.59 ± 0.27		−1.03 ± 0.28		−0.51 ± 0.32		
Teng et al. (2010a)	−2.63 ± 0.06						−0.31 ± 0.05			
Li et al. (2010)									−0.26 ± 0.07 −0.29 ± 0.09	−0.22 ± 0.07 −0.21 ± 0.09
Bourdon et al. (2010)	−2.60 ± 0.10	−0.16 ± 0.12	−0.16 ± 0.11							
Teng et al. (2010b)	−2.61 ± 0.08					−0.30 ± 0.09	−0.33 ± 0.05			

Errors stand for 2 standard deviation. *, δ^{56}Fe and error are calculated by assuming $\delta^{56}Fe = \delta^{57}Fe \times 2/3$ and error of δ^{56}Fe = error of $\delta^{57}Fe \times 2/3$.
The USGS whole rock standard data measured in UIUC laboratory is from Huang et al. (2009b).

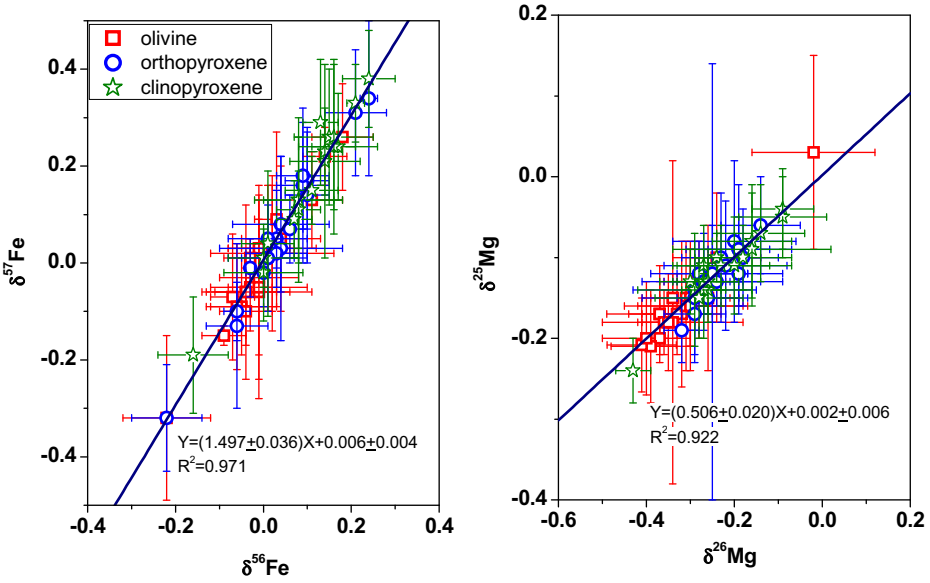

Fig. 2. Three isotope plots of Fe and Mg isotopes for minerals from the LHLS peridotite xenoliths. The slopes of δ^{56}Fe vs. δ^{57}Fe and δ^{26}Mg vs. δ^{25}Mg are 1.497 ± 0.036 and 0.506 ± 0.020, respectively, consistent with the values calculated from equilibrium and kinetic mass-dependent isotope fractionation lines (Young et al., 2002).

ranging from −0.09‰ to 0.11‰, opx from −0.09‰ to 0.10‰, and cpx from 0.00‰ to 0.17‰, respectively. δ^{56}Fe of minerals from LHLS5 and LHLS16 were replicated by digestion of different mineral grain aliquots showing good reproducibility. LHLS6 olivine is isotopically light with a δ^{56}Fe of -0.22 ± 0.10‰, while LHLS5 and LHLS16 olivines are heavier with δ^{56}Fe of 0.14 ± 0.05‰ and 0.18 ± 0.07‰, respectively. Following the behavior of olivine, opx and cpx of LHLS6 are also light (δ^{56}Fe of -0.22 ± 0.08‰ and -0.16 ± 0.08‰, respectively) while opx and cpx of LHLS5 and LHLS16 are heavy (δ^{56}Fe ranging from 0.21‰ to 0.24‰). The average δ^{56}Fe of all olivines is -0.01 ± 0.18‰ (2SD, $n = 18$), opx is 0.04 ± 0.20‰, and cpx is 0.10 ± 0.19‰. Calculated whole rock isotopic compositions display a range of δ^{56}Fe from −0.21‰ to 0.19‰ with an average of 0.01 ± 0.17‰, consistent with δ^{56}Fe of mantle peridotite xenoliths in previous studies (Williams et al., 2005, −0.38‰ to 0.10‰; Schoenberg and Blanckenburg, 2006, −0.09‰ to 0.05‰; Weyer et al., 2005, 2007, −0.02‰ to 0.07‰; Weyer and Ionov, 2007, −0.43‰ to 0.09‰; Zhao et al., 2010, −0.12‰ to 0.06‰). Our results also support the inference that the average of mantle peridotites may be slightly lighter in Fe isotopic composition relative to the average of mid-ocean ridge basalt (MORB) and oceanic-island basalt (OIB) (~0.1‰), but similar to or lighter than many island arc basalts (IAB) (−0.04‰ to 0.14‰) (e.g., Poitrasson and Freydier, 2005; Poitrasson, 2006; Teng et al., 2008; Dauphas et al., 2009a; Schoenberg et al., 2009; Schuessler et al., 2009).

Currently fewer studies of δ^{26}Mg in high temperature samples exist than those of δ^{56}Fe; they show greater inconsistency of results for different rock or mineral standards than the Fe isotope studies. Our Mg isotope data for mantle minerals (Table 3) further reinforce this inconsistency between laboratories. δ^{26}Mg of olivines from the Lianshan lherzolites vary from −0.25‰ to −0.42‰, orthopyroxene from −0.17‰ to −0.38‰, and clinopyroxene from −0.09‰ to −0.39‰ (Table 3), and therefore do not display the 4‰ range of δ^{26}Mg observed by laser ablation MC-ICP-MS (Pearson et al., 2006). The average δ^{26}Mg of olivine is -0.34 ± 0.10‰ (2SD, $n = 18$), of opx is -0.25 ± 0.10‰, and of cpx is -0.24 ± 0.18‰. The averages and ranges of δ^{26}Mg of mantle minerals in this study agree within error with data recently reported in Yang et al. (2009) (olivine, -0.29 ± 0.19‰; opx, -0.21 ± 0.09‰; cpx, -0.22 ± 0.14‰), Handler et al. (2009) (-0.27 ± 0.14‰ for olivine), and Young et al. (2009) (-0.25 ± 0.16‰ for olivine), but are systematically heavier than the values in Chakrabarti and Jacobsen (2010) by ~0.2‰ and lighter than those reported in Wiechert and Halliday (2007). Calculated δ^{26}Mg of bulk peridotites varies from −0.22‰ to −0.38‰ with an average of -0.30 ± 0.09‰ (2SD, $n = 18$) (Table 3), also in agreement with the values reported in Yang et al. (2009) (-0.26 ± 0.16‰), Teng et al. (2010a) (-0.25 ± 0.04‰), and Bourdon et al. (2010) (-0.22 ± 0.05‰), and indistinguishable from the values of terrestrial komatiites, basalts, andesites, granodiorites, and chondrites (Norman et al., 2006; Teng et al., 2007, 2010a; Tipper et al., 2008a; Huang et al., 2009b; Dauphas et al., 2010; Bourdon et al., 2010).

5. DISCUSSION

5.1. Inter-laboratory comparison of Fe and Mg isotope data

Because variations of Fe and Mg isotopic composition in high temperature rock and mineral samples are small, it is critical to examine the inter-laboratory offsets of isotope data from different groups. Comparison of widely-studied whole rock and mono-element solution standard

Table 2
Fe isotopic data for mantle minerals.

Sample	Olivine					Orthopyroxene					Clinopyroxene					$\Delta^{56}Fe_{ol-opx}$	2SD	$\Delta^{56}Fe_{ol-cpx}$	2SD
	$\delta^{56}Fe$	2SD	$\delta^{57}Fe$	2SD	*n*	$\delta^{56}Fe$	2SD	$\delta^{57}Fe$	2SD	*n*	$\delta^{56}Fe$	2SD	$\delta^{57}Fe$	2SD	*n*				
LHLS1	0.12	0.05	0.15	0.07	4	0.11	0.04	0.21	0.04	4	0.20	0.09	0.28	0.08	4	0.01	0.09	−0.06	0.11
Repeated[1]	0.10	0.06	0.12	0.11	8	0.12	0.04	0.20	0.04	4	0.14	0.07	0.21	0.08	4				
Repeated[1]						0.08	0.04	0.11	0.06	4									
Average	0.11	0.07	0.13	0.10	12	0.10	0.05	0.17	0.10	12	0.17	0.09	0.24	0.11	8				
LHLS2	−0.01	0.07	−0.01	0.14	4	−0.03	0.06	−0.10	0.17	4	0.01	0.06	0.04	0.15	6	0.07	0.09	0.00	0.08
Repeated[1]	0.03	0.04	0.07	0.11	8	−0.09	0.03	−0.16	0.16	4									
Average	0.01	0.06	0.03	0.13	12	−0.06	0.07	−0.13	0.17	8									
LHLS3	−0.01	0.09	−0.03	0.16	4	0.03	0.01	0.05	0.10	2	0.08	0.05	0.11	0.08	4	−0.04	0.09	−0.09	0.10
LHLS4	0.03	0.05	0.09	0.18	4	0.09	0.06	0.16	0.16	2	0.08	0.10	0.13	0.13	3	−0.06	0.08	−0.05	0.11
LHLS5	0.12	0.03	0.22	0.08	4	0.23	0.01	0.28	0.08	3	0.21	0.02	0.33	0.08	3	−0.10	0.05	−0.07	0.05
Repeated[2]	0.16	0.03	0.22	0.05	4	0.24	0.03	0.39	0.15	4									
Average	0.14	0.05	0.22	0.06	8	0.24	0.02	0.34	0.16	7									
LHLS6	−0.22	0.10	−0.32	0.17	4	−0.22	0.08	−0.32	0.11	4	−0.16	0.08	−0.19	0.12	4	0.00	0.13	−0.06	0.13
LHLS7	−0.07	0.05	−0.07	0.13	4	−0.03	0.01	−0.01	0.06	3	0.00	0.09	−0.02	0.10	3	−0.04	0.05	−0.07	0.10
LHLS8	0.02	0.10	0.03	0.13	4	0.01	0.03	−0.01	0.08	3	0.15	0.02	0.26	0.14	3	0.02	0.11	−0.13	0.10
Repeated[2]						−0.02	0.04	−0.03	0.08	3									
Average						0.00	0.04	−0.02	0.07	6									
LHLS9	−0.05	0.08	−0.09	0.10	4	0.01	0.09	0.01	0.03	3	0.00	0.08	0.01	0.06	2	−0.06	0.12	−0.05	0.11
LHLS10	−0.07	0.06	−0.13	0.06	4	0.01	0.09	0.05	0.08	4	0.10	0.09	0.15	0.08	4	−0.07	0.11	−0.17	0.08
Repeated[2]	−0.05	0.05	−0.06	0.14	4						0.11	0.01	0.14	0.07	4				
Average	−0.06	0.06	−0.09	0.13	8						0.11	0.06	0.15	0.07	8				
LHLS11	−0.04	0.07	−0.06	0.05	4	0.04	0.11	0.08	0.14	4	0.14	0.08	0.21	0.20	4	−0.08	0.13	−0.18	0.11
LHLS12	−0.01	0.07	0.03	0.06	4	0.09	0.06	0.18	0.11	4	0.14	0.04	0.23	0.09	4	−0.10	0.09	−0.15	0.08
LHLS13	−0.03	0.05	−0.05	0.09	4	0.10	0.05	0.14	0.14	4	0.13	0.04	0.29	0.13	4	−0.13	0.07	−0.16	0.06
LHLS14	−0.09	0.05	−0.15	0.02	4	0.04	0.14	0.03	0.19	4	0.07	0.04	0.09	0.08	4	−0.13	0.15	−0.16	0.06
LHLS15	−0.04	0.06	−0.10	0.07	4	0.03	0.07	0.02	0.03	4	0.16	0.05	0.24	0.18	4	−0.07	0.09	−0.20	0.08
LHLS16	0.18	0.07	0.26	0.11	4	0.22	0.09	0.32	0.17	4	0.24	0.06	0.38	0.10	4	−0.03	0.10	−0.06	0.09
Repeated[2]						0.21	0.07	0.30	0.08	4									
Average						0.21	0.07	0.31	0.13	8									
LHLS17	−0.03	0.06	0.01	0.04	4	0.06	0.03	0.07	0.07	4	0.08	0.08	0.13	0.17	4	−0.09	0.07	−0.11	0.10
LHLS18	0.00	0.08	−0.02	0.23	4	0.03	0.06	0.00	0.09	4	0.16	0.09	0.26	0.15	4	−0.03	0.1	−0.16	0.12
Repeated[2]	−0.07	0.08	−0.11	0.07	4	0.00	0.05	0.03	0.19	4									
Average	−0.04	0.10	−0.06	0.18	8	0.01	0.06	0.01	0.11	8									
Mineral mean	−0.01	0.18	−0.01	0.27	18	0.04	0.20	0.06	0.30	18	0.10	0.19	0.16	0.28	18	−0.05	0.11	−0.10	0.12

Note. Repeated measurements include (1) re-analysis of same purified Fe solution in different days and (2) new digestion of the same sample. *n* stands for the number of repeated analyses by MC-ICP-MS.

Table 3
Mg isotopic data for mantle minerals.

Sample	Olivine					Orthopyroxene					Clinopyroxene					$\Delta^{26}Mg_{ol-opx}$	2SD	$\Delta^{26}Mg_{ol-cpx}$	2SD
	$\delta^{26}Mg$	2SD	$\delta^{25}Mg$	2SD	*n*	$\delta^{26}Mg$	2SD	$\delta^{25}Mg$	2SD	*n*	$\delta^{26}Mg$	2SD	$\delta^{25}Mg$	2SD	*n*				
LHLS1	−0.37	0.02	−0.20	0.02	4	−0.32	0.04	−0.19	0.04	4	−0.30	0.07	−0.13	0.04	5	−0.07	0.12	−0.06	0.13
Repeated	−0.45	0.06	−0.24	0.05	4	−0.37	0.08	−0.19	0.08	4	−0.34	0.07	−0.14	0.10	4				
Repeated											−0.39	0.07	−0.19	0.05	4				
Average	−0.41	0.10	−0.21	0.07	8	−0.34	0.08	−0.19	0.07	8	−0.35	0.10	−0.16	0.11	13				
LHLS2	−0.32	0.09	−0.17	0.09	4	−0.29	0.07	−0.17	0.06	4	−0.26	0.03	−0.14	0.04	4	−0.01	0.17	−0.06	0.18
Repeated	−0.40	0.07	−0.18	0.01	4	−0.38	0.09	−0.18	0.02	6	−0.33	0.07	−0.17	0.05	6				
Average	−0.34	0.12	−0.17	0.08	8	−0.33	0.12	−0.17	0.04	10	−0.32	0.13	−0.16	0.07	10				
LHLS3	−0.30	0.12	−0.16	0.08	6	−0.29	0.12	−0.15	0.07	6	−0.09	0.07	−0.04	0.05	4	−0.01	0.17	−0.21	0.14
LHLS4	−0.37	0.12	−0.17	0.06	4	−0.26	0.07	−0.15	0.02	4	−0.43	0.04	−0.24	0.04	4	−0.11	0.14	0.06	0.13
LHLS5	−0.39	0.09	−0.21	0.07	4	−0.28	0.11	−0.12	0.04	4	−0.29	0.13	−0.14	0.07	4	−0.14	0.15	−0.13	0.16
Repeated	−0.45	0.04	−0.24	0.02	4														
Average	−0.42	0.10	−0.23	0.06	8														
LHLS6	−0.26	0.11	−0.12	0.12	5	−0.25	0.16	−0.13	0.27	3	−0.09	0.10	−0.05	0.05	4	0.00	0.21	−0.15	0.14
Repeated	−0.22	0.09	−0.10	0.05	4														
Average	−0.25	0.10	−0.10	0.08	9														
LHLS7	−0.31	0.06	−0.15	0.02	4	−0.20	0.14	−0.08	0.10	4	−0.16	0.09	−0.08	0.07	4	−0.11	0.15	−0.15	0.11
LHLS8	−0.29	0.07	−0.13	0.03	4	−0.18	0.07	−0.10	0.06	4	−0.14	0.10	−0.07	0.06	4	−0.11	0.11	−0.15	0.12
Repeated						−0.19	0.10	−0.10	0.06	4									
Average						−0.18	0.08	−0.10	0.06	8									
LHLS9	−0.34	0.07	−0.15	0.03	4	−0.19	0.10	−0.12	0.04	4	−0.16	0.18	−0.09	0.07	4	−0.15	0.12	−0.18	0.19
LHLS10	−0.41	0.08	−0.21	0.06	4	−0.17	0.17	−0.08	0.08	3	−0.20	0.12	−0.10	0.05	3	−0.22	0.14	−0.23	0.14
Repeated						−0.21	0.07	−0.10	0.08	3	−0.16	0.12	−0.09	0.05	3				
Average						−0.19	0.12	−0.09	0.08	6	−0.18	0.11	−0.10	0.04	6				
LHLS11	−0.37	0.07	−0.17	0.04	4	−0.27	0.09	−0.13	0.06	4	−0.27	0.05	−0.14	0.02	4	−0.10	0.11	−0.1	0.09
LHLS12	−0.33	0.05	−0.17	0.03	4	−0.23	0.09	−0.10	0.08	4	−0.20	0.13	−0.11	0.06	5	−0.10	0.10	−0.13	0.14
LHLS13	−0.33	0.05	−0.17	0.05	4	−0.25	0.08	−0.12	0.06	4	−0.24	0.05	−0.10	0.03	4	−0.08	0.09	−0.09	0.07
LHLS14	−0.30	0.09	−0.15	0.06	4	−0.19	0.07	−0.09	0.04	4	−0.27		−0.11		1	−0.11	0.11	−0.03	0.09
LHLS15	−0.36	0.06	−0.18	0.04	4	−0.24	0.10	−0.13	0.03	4	−0.23	0.11	−0.11	0.05	4	−0.12	0.12	−0.13	0.13
LHLS16	−0.44	0.09	−0.22	0.05	4	−0.22	0.14	−0.11	0.08	4	−0.29	0.11	−0.15	0.05	4	−0.10	0.16	−0.03	0.13
Repeated	−0.37	0.07	−0.19	0.09	4						−0.26	0.09	−0.15	0.05	4				
Repeated	−0.32	0.07	−0.17	0.02	4														
Average	−0.37	0.12	−0.19	0.06	12						−0.28	0.10	−0.15	0.05	8				
LHLS17	−0.28	0.02	−0.14	0.06	4	−0.27	0.06	−0.13	0.04	4	−0.27	0.07	−0.13	0.07	4	−0.01	0.06	−0.01	0.07
LHLS18	−0.31	0.14	−0.16	0.08	4	−0.29	0.14	−0.14	0.05	4	−0.26	0.07	−0.13	0.04	4	−0.02	0.20	−0.05	0.16
Mineral mean	−0.34	0.10	−0.17	0.06	18	−0.25	0.10	−0.12	0.06	18	−0.24	0.18	−0.12	0.09	18	−0.09	0.12	−0.10	0.15

Note. Repeated measurements are new digestion of the same sample.

Table 4
Magnesium and iron isotope composition of peridotite xenoliths from east central China.

Sample	Mg#	T (°C)	P (kbar)	Mineral mode (wt.%)				δ^{26}Mg	δ^{25}Mg	δ^{56}Fe	δ^{57}Fe
				ol	opx	cpx	sp				
LHLS1	90.1	916	10.7	56.3	27.0	14.4	1.8	−0.38	−0.20	0.11	0.15
LHLS2	90.8	918	3.5	71.4	19.1	8.9	1.0	−0.34	−0.16	0.00	0.00
LHLS3	89.0	880	12.2	59.4	23.2	14.9	2.3	−0.26	−0.14	0.01	0.01
LHLS4	90.1	966	9.6	62.7	24.5	12.5	1.2	−0.35	−0.17	0.05	0.11
LHLS5	89.3	1021	12.1	73.5	17.1	8.9	0.6	−0.38	−0.20	0.15	0.24
LHLS6	89.7	973	10.9	59.7	23.1	15.0	1.9	−0.22	−0.10	−0.21	−0.29
LHLS7	89.7	957	11.5	65.6	17.7	14.1	2.1	−0.26	−0.12	−0.05	−0.05
LHLS8	89.8	887	12.1	59.5	23.8	14.8	1.7	−0.24	−0.11	0.00	0.00
LHLS9	90.4	993	10.8	57.9	24.8	16.1	1.5	−0.27	−0.13	−0.03	−0.05
LHLS10	89.6	964	11.8	53.2	27.9	16.3	2.0	−0.30	−0.15	−0.01	−0.01
LHLS11	91.0	960	10.3	64.3	27.3	7.0	0.8	−0.33	−0.15	0.00	0.00
LHLS12	91.2	877	7.6	73.3	18.3	7.5	0.5	−0.30	−0.15	0.02	0.07
LHLS13	91.2	971	12.2	67.1	24.5	6.9	0.8	−0.30	−0.15	0.01	0.02
LHLS14	90.0	908	10.9	60.3	27.7	11.0	1.7	−0.26	−0.13	−0.04	−0.07
LHLS15	89.6	980	12.2	54.2	29.6	15.0	1.1	−0.30	−0.15	0.01	−0.01
LHLS16	89.2	1027	12.3	70.2	22.2	7.5	0.1	−0.33	−0.17	0.19	0.28
LHLS17	90.3	980	11.5	57.4	28.6	12.6	1.7	−0.27	−0.13	0.01	0.04
LHLS18	89.7	970	11.3	54.7	27.7	17.1	–	−0.29	−0.15	0.01	0.01
Average								−0.30	−0.15	0.01	0.03
2σ								0.09	0.05	0.17	0.25

Mg# is from Reisberg et al. (2005). Temperature and pressure were calculated using two pyroxene barometers and thermometers in Putirka (2008).

data provides a good way to reveal inter-laboratory analytical discrepancies. Three USGS whole rock standards (BIR-1, AGV-1, and BCR-2) and one in-house pure Fe solution standard (ETH hematite) were measured in the UIUC laboratory for δ^{56}Fe (Table 1). These data show excellent agreement with literature values, suggesting that inter-laboratory biases for Fe isotopes are negligible.

In contrast, considerable discrepancies in Mg isotope data exist for whole rock standards reported in the literature (Table 1). For the pure Mg solution CAM-1, average δ^{26}Mg of 44 measurements from the UIUC laboratory is -2.63 ± 0.11‰, consistent with other literature values (e.g., Galy et al., 2001, 2003; Tipper et al., 2006a,b, 2008a,b; Yang et al., 2009; Young et al., 2009; Bourdon et al., 2010). Data for whole rock standards show more variations. For example, our two analyses of DTS-1 (a dunite standard) yielded δ^{26}Mg of -0.30 ± 0.16‰ and -0.37 ± 0.06‰, respectively (Huang et al., 2009b), in agreement with the values reported in Yang et al. (2009) (-0.30 ± 0.05‰), Wombacher et al. (2009) (-0.25 ± 0.08‰), and Teng et al. (2010b) (0.30 ± 0.09), but quite different from that (-1.03 ± 0.28‰) in Chakrabarti and Jacobsen (2010). δ^{26}Mg of BCR-1, BHVO-1, and PCC-1 reported in Chakrabarti and Jacobsen (2010) are also systematically lighter than the values in other studies by 0.2‰ (Table 1). Two granite standards from the UIUC laboratory (GA, -0.34 ± 0.15‰; and GSN, -0.24 ± 0.23‰) are close to the values reported in Li et al. (2010) but our GA data are different from the δ^{26}Mg reported in Bolou-Bi et al. (2009) (-0.75 ± 0.14‰). Our BCR-1 and BCR-2 data are consistent with the values in Young and Galy (2004) and Teng et al. (2007), but slightly lighter than those reported in Bizzarro et al. (2005), Tipper et al. (2008a), Wombacher et al. (2009), and Bourdon et al. (2010), although all the reported data are still consistent within error (2SD).

Because the δ^{26}Mg of San Carlos olivine reported in the literature showed large variations from −0.06‰ to −0.73‰ (Pearson et al., 2006, −0.58‰ and −0.64‰; Wiechert and Halliday, 2007, −0.06‰; Teng et al., 2007, −0.62‰ and −0.73‰; Handler et al., 2009, −0.17‰; Huang et al., 2009b, −0.27‰), a homogenized standard was recently made by handpicking and powdering ~50 g of San Carlos olivine to eliminate possible isotopic heterogeneity (Chakrabarti and Jacobsen, 2010). This standard was measured in three laboratories and the reported δ^{26}Mg still ranged from −0.19‰ to −0.55‰ (Young et al., 2009, −0.19‰; Chakrabarti and Jacobsen, 2010, −0.55‰; Liu et al., 2010, −0.27‰). This indicates that the inter-laboratory discrepancies for the whole rock and olivine standards do not reflect Mg isotopic heterogeneity but analytical artifacts, resulting from standard solution storage issues, matrix effects, low yields of chemical procedures, or a combination of the above. This makes inter-laboratory comparisons for Mg isotope data currently difficult. More analyses of whole rock and mineral standards and inter-laboratory calibration are needed in order to advance this tool.

5.2. Inter-mineral Fe and Mg isotope fractionation

Recent advances in analytical methods for high precision Mg and Fe isotopic measurements and theoretical calculations of equilibrium fractionation at high temperatures allow better understanding of inter-mineral isotopic fractionation in mantle peridotites. $\Delta^{56}Fe_{ol-opx}$ of 18 samples

varies from 0.07‰ to −0.13‰ with an average of -0.05 ± 0.11‰ (2SD) while $\Delta^{56}Fe_{ol-cpx}$ in this study varies from 0.00‰ to −0.20‰ with an average of -0.10 ± 0.12‰ (2SD, $n = 18$) (Table 2 and Fig. 3). The histogram of $\delta^{56}Fe$ indicates that olivine has a slightly lighter $\delta^{56}Fe$ (or $\delta^{57}Fe$) than clinopyroxene, but similar $\delta^{56}Fe$ (or $\delta^{57}Fe$) to orthopyroxene (Fig. 4), consistent with previous studies (e.g., Beard and Johnson, 2004; Williams et al., 2005; Weyer and Ionov, 2007; Zhao et al., 2010). Although these isotopic differences generally agree with theoretical prediction of inter-mineral equilibrium fractionation factors (e.g., $\Delta^{56}Fe_{ol-cpx} = -0.09$‰ and $\Delta^{56}Fe_{ol-opx} = 0.03$‰ at 1000 °C, Polyakov and Mineev, 2000), it is still unclear whether these isotopic offsets reflect inter-mineral equilibrium or disequilibrium as a consequence of open system processes (Beard and Johnson, 2004; Williams et al., 2005; Zhao et al., 2010).

Because equilibrium isotope fractionation factor between mantle mineral pairs is generally small at high temperature, mantle minerals in equilibrium should match in isotopic variations. Therefore, isotopic equilibrium between mineral pairs can be assessed using plots of $\delta^{56}Fe$ vs. $\delta^{56}Fe$, where minerals in equilibrium should fall on a line with a slope of ~1 (e.g., Beard and Johnson, 2004; Williams et al., 2005; Zhao et al., 2010) but with different intercept reflecting the fractionation factor. Fe and Mg isotope data for mantle minerals compiled from the literature and this study are shown in Fig. 3. $\delta^{56}Fe_{ol}$ are well correlated with both $\delta^{56}Fe_{opx}$ and $\delta^{56}Fe_{cpx}$ (Fig. 3A and B). Linear regressions give equations of $Y = (1.02 \pm 0.25)X + 0.05 \pm 0.03$ and $Y = (1.00 \pm 0.22)X + 0.08 \pm 0.02$ for the Fe isotope data trend of olivine–opx ($n = 52$) and olivine–cpx ($n = 56$) pairs, respectively. Therefore, we argue that Fe isotopes are likely in equilibrium among most olivine, cpx, and opx on a hand sample length scale.

Although there is a hint of Mg isotopic fractionation between olivines and pyroxenes (Figs. 3, 4 and Table 3), $\delta^{26}Mg$ of mantle minerals are indistinguishable within current analytical errors of ~0.1‰. $\Delta^{26}Mg_{ol-opx}$ of most samples varies from 0‰ to −0.22‰ with an average value of -0.09 ± 0.11‰ ($n = 18$, 2SD), and $\Delta^{26}Mg_{ol-cpx}$ from 0.06‰ to −0.23‰ with an average of -0.10 ± 0.15‰ (Table 3). These offsets agree with those reported in Handler et al. (2009), Yang et al. (2009), and Young et al. (2009) (Fig. 3), and with the theoretical prediction

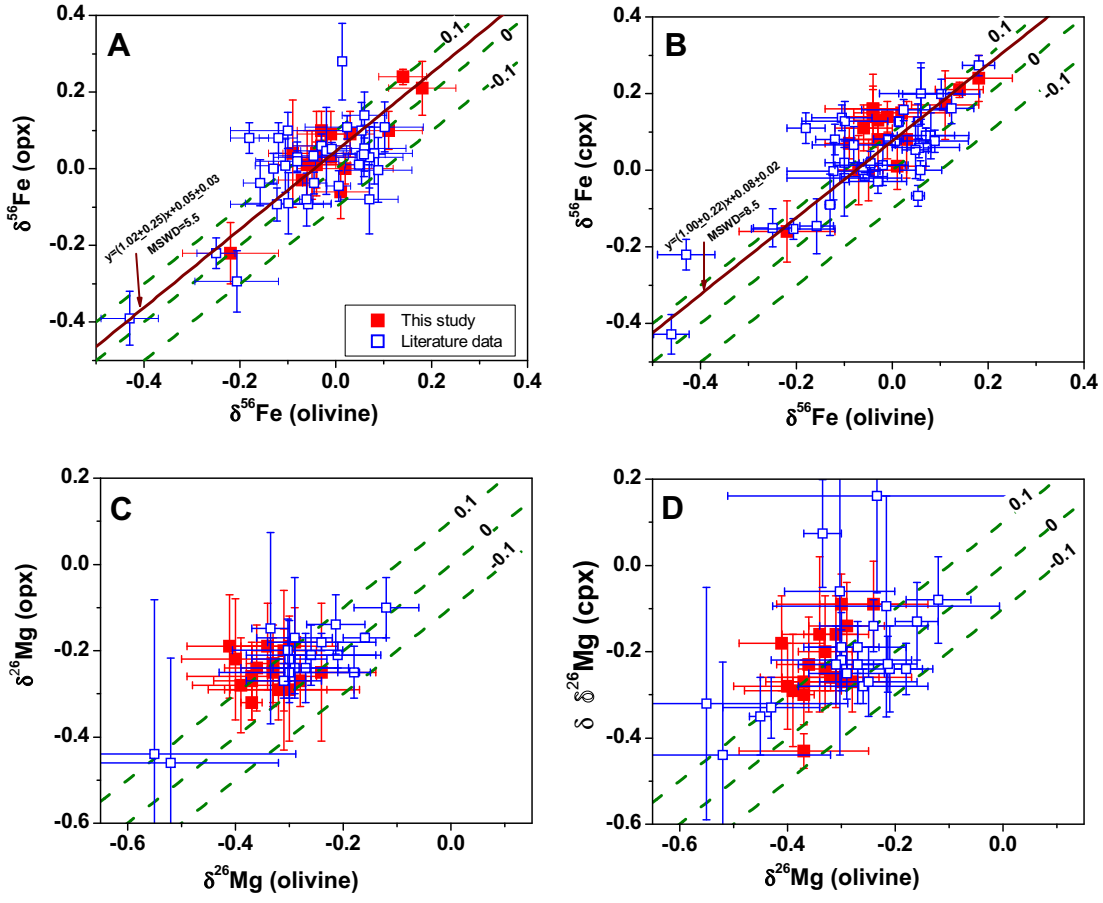

Fig. 3. Fe and Mg isotope fractionation between minerals from the Lianshan peridotite xenoliths. Literature data of $\delta^{56}Fe$ are from Zhu et al. (2002), Beard and Johnson (2004), Williams et al. (2005),Weyer et al. (2007), Weyer and Ionov (2007), and Zhao et al. (2010); Literature data of $\delta^{26}Mg$ are from Yang et al. (2009), Handler et al. (2009), Young et al. (2009), and Chakrabarti and Jacobsen (2010). The error bars stand for 2SD. $\delta^{56}Fe_{ol}$ shows a linear correlation with $\delta^{56}Fe_{opx}$ and $\delta^{56}Fe_{cpx}$ with slopes close to unity. The functions of dash lines are $Y = X$, or $Y = X \pm 0.1$. The correlations between $\delta^{56}Fe$ of minerals in (A and B) were linearly fitted by a least squares method. Errors given reflect 2σ.

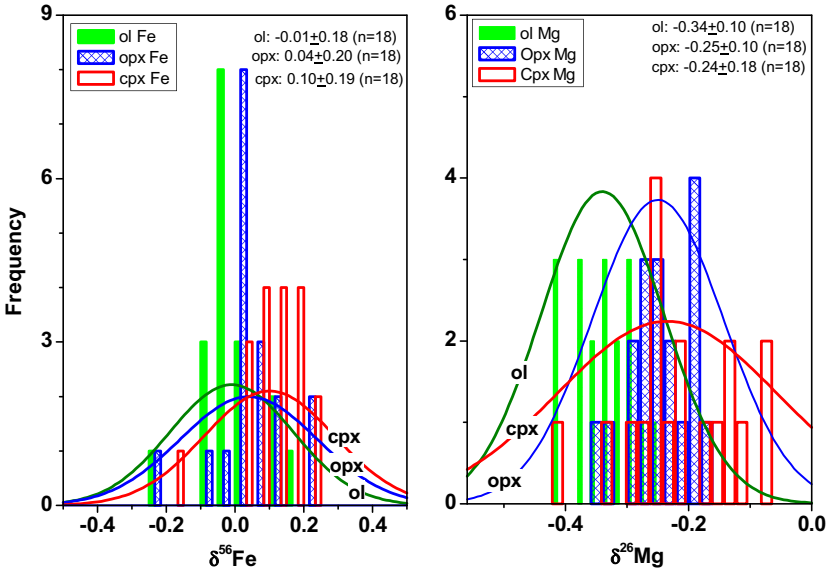

Fig. 4. Histograms showing inter-mineral Fe and Mg isotope fractionations. The mineral curves follow standard Gaussian distribution function: $f(x) = \frac{1}{\sigma\sqrt{2\pi}} \exp(-\frac{(x-\mu)^2}{2\sigma^2})$, where μ is the average and σ is the error.

for inter-mineral equilibrium fractionations at high temperatures (Young et al., 2009; Schauble, 2011) (Fig. 5). It is likely that such slight but systematic fractionations suggest Mg isotopic equilibrium between minerals for most samples of this study, consistent with the implications of Fe isotope observations.

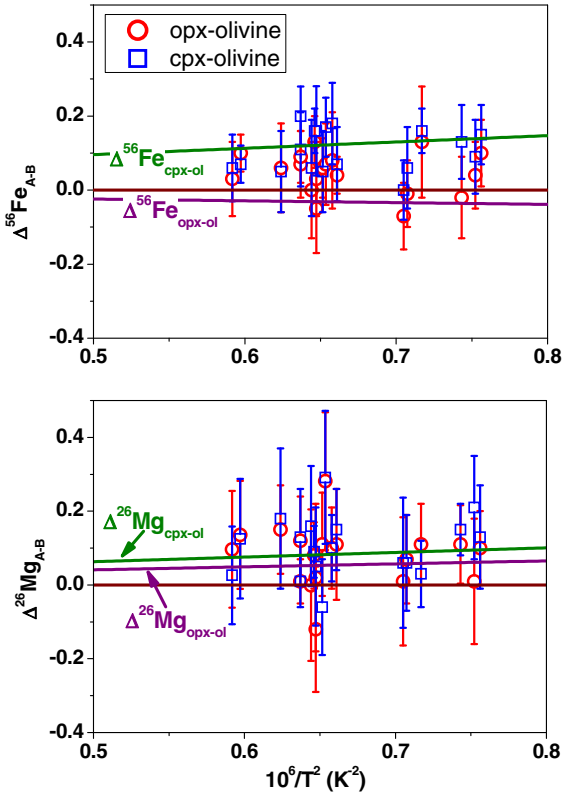

Fig. 5. Variation of Fe and Mg isotope fractionation between mantle minerals with equilibrium temperatures calculated using the two-pyroxene thermometer from Putirka (2008). The equilibrium isotope fractionation curves for Fe and Mg isotopes are from Polyakov and Mineev (2000) and Young et al. (2009), respectively.

The conclusion that mantle minerals are commonly in Fe and Mg isotopic equilibrium is not surprising given the fact that most mantle minerals are in oxygen isotope equilibrium and span a narrow range in $\delta^{18}O$ (Mattey et al., 1994; Hoefs, 1997; Eiler, 2001) and that the diffusion coefficient of oxygen is slower than that of iron and magnesium in mantle minerals (e.g., Gérard and Jaoul, 1989). Although a few studies presented variable oxygen isotope data showing inter-mineral isotopic disequilibrium, these peridotite samples are rare and normally exhibit elemental disequilibrium and intra-crystal zoning probably reflecting strong fluid–rock interaction (such as the polymict peridotite xenoliths from the Kaapvaal Craton, South Africa; Zhang et al., 2000). However, this is not the case for the xenoliths studied for Fe–Mg–Ca isotopes (such as those from East China and San Carlos). Isotopic equilibrium can be obtained by diffusion in a few million years or by dissolution and re-precipitation in considerably less time (e.g., Williams et al., 2005).

5.3. Implications for mineral thermometers and barometers

Inter-mineral isotopic fractionation provides important constraints on the applications of mineral thermometers and barometers. Complete chemical equilibrium between mineral pairs is the prerequisite of mineral thermometers and barometers. If elemental and isotopic equilibrium between mantle minerals is disturbed by partial melting or metasomatism, isotopic equilibrium should be approached via kinetic processes (e.g., chemical diffusion) much faster than elemental equilibrium (Lesher, 1990, 1994; Laan et al., 1994). Therefore, theoretically, any disequilibrium

indicated by non-equilibrium partitioning of major element isotopes (such as O, Mg, and Fe) between minerals would provide a demonstration of elemental disequilibrium, which in turn strongly suggests that the calculated equilibrium temperatures and pressures would not be reliable. Therefore, if Fe isotopic disequilibrium exists among mantle minerals, equilibrium pressures and temperatures cannot be expected to be extracted from mineral thermometers and barometers (e.g., Zhao et al., 2010).

Density functional calculations, based on differences in metal–O bonding environments in mantle minerals, have been used to provide quantitative estimates of equilibrium fractionation factors for Mg and Ca isotopes between minerals from San Carlos peridotite xenoliths (Young et al., 2009; Huang et al., 2010b). This has led to the proposal that Mg isotope inter-mineral fractionations could be used as a new geo-thermometer (Young et al., 2009). Similarly, San Carlos minerals exhibit slight Fe isotopic fractionation ($\Delta^{56}Fe_{ol-cpx} = -0.08‰$; $\Delta^{56}Fe_{ol-opx} = 0.01‰$) (Weyer et al., 2007), which agrees well with the data in our study and theoretical prediction of equilibrium fractionation (Polyakov and Mineev, 2000). However, measured Ca and Mg isotopic offsets between San Carlos opx and cpx is significantly larger than predictions based on density functional calculations at normal upper mantle temperatures (Young et al., 2009; Huang et al., 2010b). Geochemical studies of the San Carlos peridotites show complete chemical equilibrium with a reasonable two-pyroxene temperature around 1000 °C (Galer and O'Nions, 1989), which is significantly higher than the equilibrium temperature calculated from olivine–opx and olivine–cpx Mg isotope thermometers (300–400 °C) (Young et al., 2009). Furthermore, at 1000 °C, $\Delta^{26}Mg_{cpx-opx}$ predicted from density functional calculation is 0.027‰ (Young et al., 2009), close to the average of $\Delta^{26}Mg_{cpx-opx}$ in LHLS samples (0.015‰) (Fig. 5), but much smaller than the $\Delta^{26}Mg_{cpx-opx}$ (0.28‰) of San Carlos peridotites measured in Young et al. (2009). This indicates a clear discrepancy between elemental and isotopic thermometers for mantle peridotites and raises questions about the results of isotopic thermometers.

There are three explanations for the temperature discrepancy. First, it could reflect the fact that the density functional calculations only provide qualitative or semi-quantitative estimates of partitioning of stable isotopes between mantle minerals (Young et al., 2009; Huang et al., 2010b), and thus may not be accurate enough to quantify equilibrium fractionation factors of Mg isotopes. Second, it is possible that San Carlos peridotites measured in Young et al. (2009) are indeed in isotopic disequilibrium, and they are different from the San Carlos samples studied by Galer and O'Nions (1989) and Weyer et al. (2007). Measurement of major element and Mg isotopic compositions for minerals from the same San Carlos peridotite is necessary to address this possibility. And third, the $\delta^{26}Mg$ of San Carlos cpx in Young et al. (2009) may not be representative or accurate. $\delta^{26}Mg$ of cpx in the most recent studies range from −0.06‰ to −0.39‰ (Handler et al., 2009; Yang et al., 2009; and this study), while two San Carlos cpx determined in Young et al. (2009) exhibit significantly higher $\delta^{26}Mg$ (0.16‰ and 0.13‰). Clearly, successful application of Mg isotope thermometry requires more accurate and precise Mg isotope data for mantle minerals in future studies.

5.4. Fe and Mg isotope compositions of the upper mantle

Investigation of peridotite xenoliths provides a direct characterization of the lithospheric mantle avoiding the issue of isotopic fractionation produced during magma generation, evolution or even weathering processes. Fig. 6 shows Fe and Mg isotopic compositions of mantle minerals and bulk peridotites calculated based on mineral modes. We estimate the $\delta^{26}Mg$ of the BSE to be $-0.30 \pm 0.09‰$ (2SD), based on the average of 18 peridotites measured here. Although there remain inter-laboratory discrepancies of Mg isotope data as shown by standard analyses (Table 1), there is generally good agreement between laboratories for the ^{26}Mg of the BSE, with our value being within error of those of Handler et al. (2009) ($-0.27 \pm 0.14‰$), Yang et al. (2009) ($-0.26 \pm 0.16‰$), Dauphas et al. (2010) ($-0.28 \pm 0.04‰$), Teng et al. (2010a) ($-0.25 \pm 0.07‰$), and Bourdon et al. (2010) ($-0.23 \pm 0.11‰$). However, our value is significantly heavier than that of Chakrabarti and Jacobsen (2010) (−0.54‰). Our results do not exhibit any resolvable difference with the $\delta^{26}Mg$ of chondrites (−0.14‰ to −0.36‰) recently reported in Young et al. (2009), Teng et al. (2010a), and Bourdon et al. (2010), likely implying a chondritic Mg isotopic composition of the BSE.

$\delta^{56}Fe$ values of whole rocks range from 0.19‰ to −0.21‰. Excluding the few samples which may be affected by metasomatism (see discussion below), the average $\delta^{56}Fe$ is $0.01 \pm 0.08‰$ (2SD, $n = 15$). This value agrees well with those of previous studies of mantle peridotites and

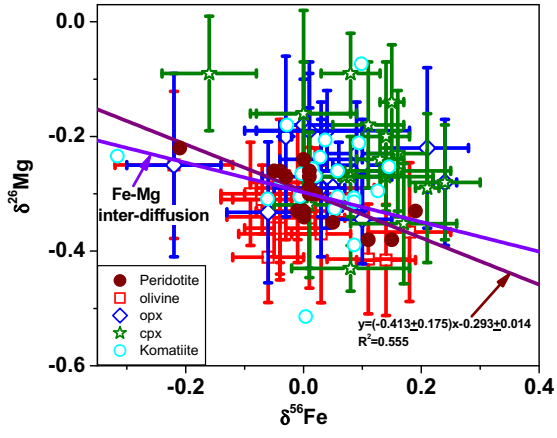

Fig. 6. $\delta^{56}Fe$ and $\delta^{26}Mg$ of olivine, opx, cpx, and bulk peridotites. $\delta^{56}Fe$ shows a larger range than $\delta^{26}Mg$, suggesting that Fe isotopes of peridotites are more easily fractionated than Mg isotopes. Komatiite data are from Dauphas et al. (2010), which are plotted for a comparison with peridotites. The slope of Fe–Mg inter-diffusion line is −0.258, which was calculated assuming $\beta_{Fe}/\beta_{Mg} = 1$ and Mg# = 89.7 (from LHLS6). The negative correlation between $\delta^{56}Fe$ and $\delta^{26}Mg$ of bulk rocks was linearly fitted by a least squares method. Errors on slope and intercept reflect 2δ.

chondrites (Poitrasson et al., 2004; Williams et al., 2004, 2005; Weyer et al., 2005, 2007; Schoenberg and Blanckenburg, 2006; Weyer and Ionov, 2007), supporting the premise that the BSE has a chondritic Fe isotopic composition (Weyer and Ionov, 2007; Weyer et al., 2007).

5.5. Variation of Fe and Mg isotopic composition in mantle peridotites

Substantial variations of δ^{56}Fe between different peridotite xenoliths (up to 0.4‰) are observed in this study. We assess the two mechanisms suggested in previous studies, partial melting and metasomatism to explain this variation. Two high δ^{56}Fe samples (LHLS5 and LHLS16) have high total FeO contents, La/Yb, and high equilibration temperatures relative to other samples (Figs. 7 and 8). Although these two samples also have lower Mg# than most other xenoliths, δ^{56}Fe of the bulk Lianshan samples overall does not show a systematic variation with Mg# (Fig. 7). This suggests that partial melting of fertile mantle does not cause significant Fe isotopic fractionation in the Lianshan peridotites.

Instead, the heavy δ^{56}Fe in LHLS5 and LHLS16 probably result from reaction between peridotites and evolved, silica-undersaturated Fe-rich melts providing the observed coupling of high δ^{56}Fe with high FeO content and La/Yb. This process has been proposed to produce low Mg#, high FeO content, and high La/Yb (Ionov et al., 2005) and was referred to as E-1 type metasomatism in Weyer and Ionov (2007). Our data further show that its influence on Mg isotope ratios cannot be clearly resolved with current analytical precision (±0.1‰) (Fig. 8), either because the metasomatic melt has similar Mg isotopic composition to that of the peridotites or because isotopic variation caused by metasomatism is diluted by the high Mg content of peridotites. As discussed in Weyer and Ionov (2007), melts with high FeO content and heavy Fe isotopes can be produced by partial melting of fertile mantle and magma evolution in the mantle via fractional crystallization and melt–peridotite interaction. However, unlike the samples that experienced the E-1 type metasomatism in Weyer and Ionov (2007), LHLS5 and LHLS16 do not have very high CaO/Al_2O_3 and cpx/opx (Fig. 7).

The coupling of high δ^{56}Fe and high La/Yb in LHLS5 and LHLS16 contrasts with the negative correlation between δ^{57}Fe and La/Yb in cpx recently observed in Cenozoic xenoliths from Hannuoba and Hebi in the NCC (Fig. 1) (Zhao et al., 2010). This may reflect a different role of metasomatism in modifying geochemistry of peridotites from these two locations. The lack of sulfides and low Re (0.016–0.15 ppb) and Os contents (0.14–3.78 ppb) in LHLS xenoliths suggests extensive melt percolation (Reisberg et al., 2005), while Hannuoba samples have abundant sulfides and high Re (0.04–0.29 ppb) and Os contents (1.88–4.65 ppb) (Gao et al., 2002), arguing that metasomatism was a less pervasive process than in the Lianshan samples.

LHLS6 has lower bulk δ^{56}Fe (−0.21‰) than the other samples. Notably $^{187}Os/^{188}Os$, CaO/Al_2O_3, Mg#, La/Yb,

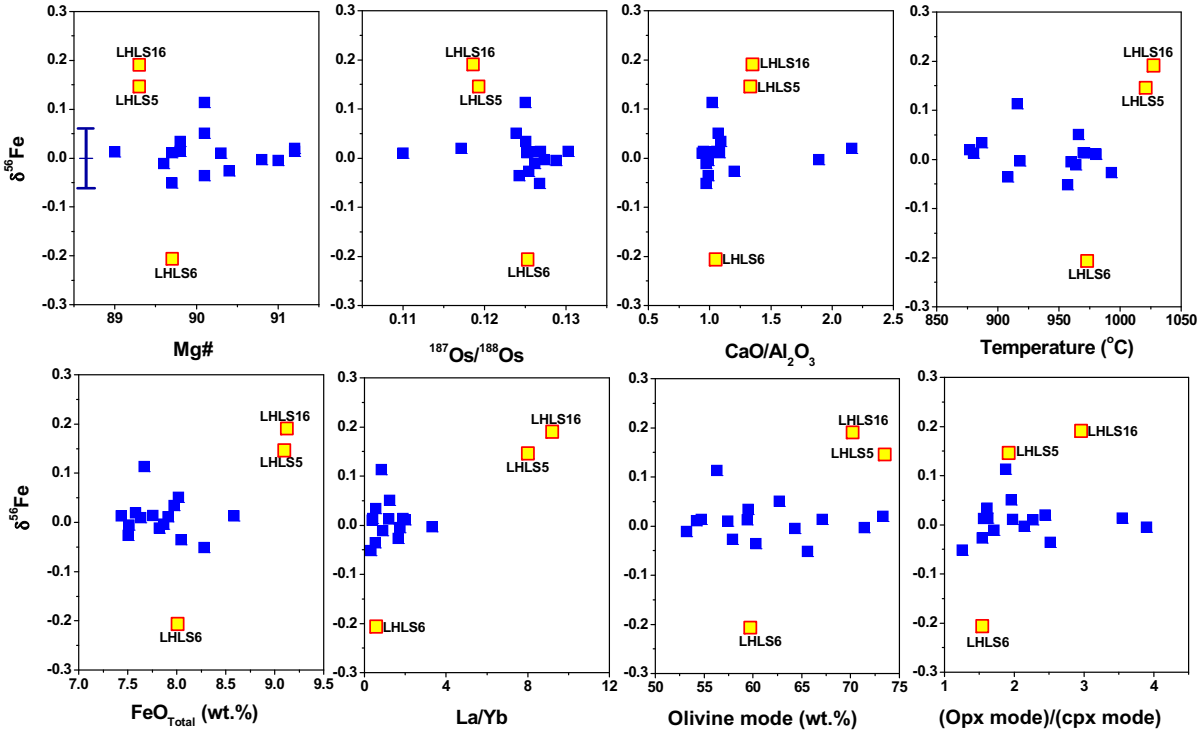

Fig. 7. Variations of δ^{56}Fe of the Lianshan peridotites with Mg#, $^{187}Os/^{188}Os$, CaO/Al_2O_3, temperature, total FeO content, La/Yb, mode of olivine, and (opx mode)/(cpx mode). Data source is Reisberg et al. (2005). Error bar for δ^{56}Fe is about 0.06‰ (2SD) based on the average of errors for all mineral analyses.

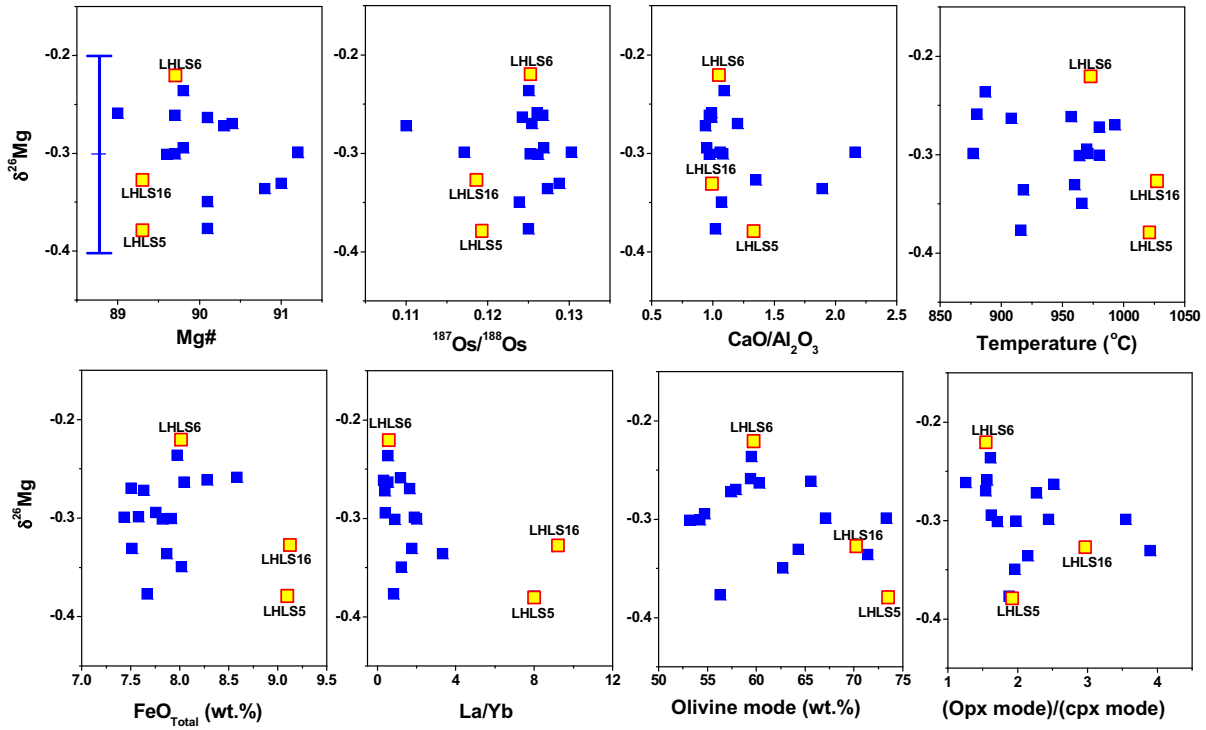

Fig. 8. Variations of δ^{26}Mg of the Lianshan peridotites with Mg#, ^{187}Os/^{188}Os, CaO/Al_2O_3, temperature, total FeO content, La/Yb, mode of olivine, and (opx mode)/(cpx mode). Data source is Reisberg et al. (2005). Error bar for δ^{26}Mg is about 0.1‰ (2SD) based on the average of errors for all mineral analyses.

total FeO content, equilibrium temperature, olivine mode, and opx/cpx of LHLS6 are not clearly different from the values of other samples having normal δ^{56}Fe (Fig. 7), suggesting that the low δ^{56}Fe may not be due to partial melting of the fertile mantle leaving depleted and isotopically light residue behind. Based on mass-balance calculation, Williams et al. (2005) also argue that such light isotopic signatures are unlikely to be due to metasomatism by recycled crustal components or fluids from subducted slabs. Therefore, we propose that the low δ^{56}Fe in LHLS6 could result from diffusion of light Fe isotopes from Fe-rich melt into the peridotite during melt percolation, a process similar to the E-2 type metasomatism proposed by Weyer and Ionov (2007) to explain a few samples with light Fe isotope compositions. The LHLS6 olivine also has a heavier Mg isotopic composition than other samples as confirmed by repeated analyses (Fig. 8 and Table 3). This is similar to the recent observation by Dauphas et al. (2010) in which olivine minerals from Alexo komatiites have lighter Fe isotopic composition but slightly heavier Mg isotopic composition than the average bulk komatiites.

The bulk δ^{56}Fe of LHLS lherzolites is roughly negatively correlated with δ^{26}Mg (Fig. 6). This correlation may not be produced by partial melting because the Lianshan lherzolites have normal Mg# ranging from 89.0 to 91.2 with an average of 90.0. Instead, it is consistent with the prediction from theoretical modeling of isotope fractionation in olivine due to Fe–Mg inter-diffusion (Dauphas et al., 2010). During percolation of Fe-rich melt in the upper mantle, it is likely that light Fe isotopes preferentially diffuse into mantle minerals, while light Mg isotopes preferentially diffuse into the melt. The slope defined by the correlation between δ^{56}Fe and δ^{26}Mg is sensitive to the mass dependent isotope fractionation factor (β) and relative abundances of Fe and Mg (or Mg#) in the peridotites. Variation of Fe and Mg isotopes of peridotite can be expressed as: $\frac{\delta^{56}\mathrm{Fe}}{\delta^{26}\mathrm{Mg}} \approx -\frac{\beta_{\mathrm{Fe}}(56/54-1)Mg\#}{\beta_{\mathrm{Mg}}(26/24-1)(100-\mathrm{Mg})}$. This equation is slightly modified from the one originally used in Dauphas et al. (2010) to simulate Fe–Mg isotope diffusive fractionation in an olivine with low δ^{56}Fe and slightly high δ^{26}Mg from Alexo komatiites, Canada. β_{Fe} and β_{Mg} for diffusion in silicate minerals are not experimentally determined yet. If $\beta_{\mathrm{Fe}}/\beta_{\mathrm{Mg}} = 1$ and Mg# = 89.7 (from LHLS6), Fe–Mg inter-diffusion can produce a line with slope of −0.258 (Fig. 6). If $\beta_{\mathrm{Fe}}/\beta_{\mathrm{Mg}} = 0.63$, the slope of inter-diffusion trend is same as the slope of the LHLS trend (−0.413) (Fig. 6). The greater variation in δ^{56}Fe compared with δ^{26}Mg indicates that metasomatism and kinetic processes may have a greater effect on Fe isotopes than on Mg isotopes for mantle peridotites. This could also be due to a greater dilution effect on Mg isotopes relative to Fe isotopes. However, the current analytical uncertainties (0.1‰, 2SD) and the small variation of δ^{26}Mg in peridotite in this study (−0.22‰ to −0.38‰) do not allow us to further address the hypothesis of diffusion-driven Mg isotope fractionation in mantle peridotites. More studies with higher precision Mg isotopic data are needed to improve our understanding of Mg isotopic variation in the upper mantle.

6. CONCLUSIONS

This study presents the first study combining high precision Fe and Mg isotopic data for coexisting mantle minerals in peridotite xenoliths. The following conclusions can be drawn:

(1) Although the Mg isotopic compositions of coexisting olivine, opx, and cpx are indistinguishable within current analytical uncertainties, pyroxenes statistically have slightly heavier δ^{26}Mg than olivine. Olivine has slightly lighter δ^{56}Fe than cpx but has identical δ^{56}Fe to opx, consistent with previous studies (Williams et al., 2005; Zhao et al., 2010) and theoretical calculations for inter-mineral equilibrium isotopic fractionation (Polyakov and Mineev, 2000). These observations and a positive linear correlation with a slope of unity in the δ^{56}Fe–δ^{56}Fe plot for coexisting minerals suggest inter-mineral isotopic equilibrium for both the Fe and Mg systems in most samples. Given that inter-mineral isotopic equilibrium should be reached faster than elemental equilibrium at high temperature, mineral barometers and thermometers cannot be applied to samples which show inter-mineral Fe and Mg isotope disequilibrium.

(2) δ^{56}Fe and δ^{26}Mg of bulk LHLS samples calculated using the modes of olivine, opx, and cpx range from 0.19‰ to −0.21‰ and −0.22 to −0.38‰, respectively. The average δ^{56}Fe of the peridotites studied here is 0.01 ± 0.17‰ ($n = 18$, 2SD) in agreement with previous studies (e.g., Weyer and Ionov, 2007); Similarly, the average δ^{26}Mg is -0.30 ± 0.09‰, identical with the values of the BSE estimated in several recent studies (−0.23‰ to −0.28‰) (Yang et al., 2009; Handler et al., 2009; Dauphas et al., 2010; Teng et al., 2010a; Bourdon et al., 2010). Our results suggest a chondritic Fe and Mg isotopic composition for the BSE.

(3) Although most LHLS lherzolites generally show limited variation in δ^{56}Fe, a few outliers provide evidence for metasomatic resetting and fractionation during Fe–Mg diffusive exchange. Two samples have significantly higher δ^{56}Fe than average mantle. Notably these samples have higher La/Yb, total FeO content, and equilibration temperature relative to the other peridotites in this study, likely reflecting metasomatic reaction between peridotite and Fe-rich silicate melt. One sample has lighter δ^{56}Fe and slightly heavy δ^{26}Mg relative to the average, suggesting that diffusion-driven kinetic processes may play a role in fractionating Fe and Mg isotopes in mantle peridotites. The data of this study indicate that metasomatism and kinetic processes may have greater effects on δ^{56}Fe than on δ^{26}Mg for mantle peridotites.

ACKNOWLEDGMENTS

This work is supported by NSF EAR 0609726. Work in the MC-ICPMS laboratory is supported by NSF EAR 0732481. The authors thank A. Galy for providing DSM-3 and CAM-1 solutions, Justin Glessner for the help of Fe and Mg isotope data analyses, Adam Ianno, Wang-Ye Li, Sheng-Ao Liu, Wei Yang, and Fang-Zhen Teng for comments on the early version of this paper, and Alan Boudreau for measuring major element composition for spinels. Constructive comments by Laurie Reisberg, Helen Williams, Shi-Chun Huang, Gang Yu, and an anonymous reviewer and editorial handling by Alan Brandon were highly appreciated.

APPENDIX A. SUPPLEMENTARY DATA

Supplementary data associated with this article can be found, in the online version, at doi:10.1016/j.gca.2011.03.036.

REFERENCES

Beard B. L., Johnson C. M., Skulan J. L., Nealson K. H., Cox L. and Sun H. (2003) Application of Fe isotopes to tracing the geochemical and biological cycling of Fe. *Chem. Geol.* **195**, 87–117.

Beard B. L. and Johnson C. M. (2004) Inter-mineral Fe isotope variations in mantle-derived rocks and implications for the Fe geochemical cycle. *Geochim. Cosmochim. Acta* **68**, 4727–4743.

Bizzarro M., Baker J. A., Haack H. and Lundgaard K. L. (2005) Rapid timescales for accretion and melting of differentiated planetesimals inferred from ^{26}Al–^{26}Mg chronometry. *Astrophys. J.* **632**, 41–44.

Bolou-Bi E. B., Vigier N., Brenot A. and Poszwa A. (2009) Magnesium isotope compositions of natural reference materials. *Geostand. Geoanal. Res.* **33**, 95–109.

Bourdon B., Tipper T. E., Fitoussi C. and Stracke A. (2010) Chondritic Mg isotope composition of the Earth. *Geochim. Cosmochim. Acta* **74**, 5069–5083.

Chakrabarti R. and Jacobsen S. B. (2010) The isotopic composition of magnesium in the inner Solar System. *Earth Planet. Sci. Lett.* **293**, 349–358.

Chen L.-H., Zeng G., Jiang S.-Y., Hofmann A. W., Xu X.-S. and Pan M.-B. (2009a) Sources of Anfengshan basalts: subducted lower crust in the Sulu UHP belt, China. *Earth Planet. Sci. Lett.* **286**, 426–435.

Chen L., Cheng C. and Wei Z. (2009b) Seismic evidence for significant lateral variations in lithospheric thickness beneath the central and western North China Craton. *Earth Planet. Sci. Lett.* **286**, 171–183.

Chen L., Tao W., Zhao L. and Zheng T. (2008) Distinct lateral variation of lithospheric thickness in the Northeastern North China Craton. *Earth Planet. Sci. Lett.* **267**, 56–68.

Craddock P. R. and Dauphas N. (2011) Iron isotopic compositions of geological reference materials and chondrites. *Geostand. Geoanal. Res.* **35**, 101–123.

Dauphas N., Craddock P. R., Asimow P. D., Bennett V. C., Nutman A. P. and Ohnenstetter D. (2009a) Iron isotopes may reveal the redox conditions of mantle melting from Archean to Present. *Earth Planet. Sci. Lett.* **288**, 255–267.

Dauphas N., Pourmand A. and Teng F.-Z. (2009b) Routine isotopic analysis of iron by HR-MC-ICP-MS: how precise and how accurate?. *Chem. Geol.* **267** 175–184.

Dauphas N. and Rouxel O. (2006) Mass spectrometry and natural variations of iron isotopes. *Mass Spectrom. Rev.* **25**, 515–550.

Dauphas N., Teng F.-Z. and Arndt N. T. (2010) Magnesium and iron isotopes in 2.7 Ga Alexo komatiites: mantle signatures, no evidence for Soret diffusion, and identification of diffusive

transport in zoned olivine. *Geochim. Cosmochim. Acta* **74**, 3274–3291.

Dideriksen K., Baker J. A. and Stipp S. L. S. (2006) Iron isotopes in natural carbonate minerals determined by MC-ICP-MS with a ^{58}Fe–^{54}Fe double spike. *Geochim. Cosmochim. Acta* **70**, 118–132.

Eiler J. M. (2001) Oxygen isotope variations of basaltic lavas and upper mantle rocks. *Rev. Mineral. Geochem.* **43**, 319–364.

Galer S. J. G. and O'Nions R. K. (1989) Chemical and isotopic studies of ultramafic inclusions from the San Carlos Volcanic Field, Arizona: a bearing on their petrogenesis. *J. Petrol.* **30**, 1033–1064.

Galy A., Belshaw N. S., Halicz L. and O'Nions R. K. (2001) High-precision measurement of magnesium isotopes by multiple-collector inductively coupled plasma mass spectrometry. *Int. J. Mass Spectrom.* **208**, 89–98.

Galy A., Yoffe O., Janney P., Williams R., Cloquet C., Alard O., Halicz L., Wadhwa M., Hutcheon I., Ramon E. and Carignan J. (2003) Magnesium isotope heterogeneity of the isotopic standard SRM980 and new reference materials for magnesium-isotope ratio measurements. *J. Anal. At. Spectrom.* **18**, 1352–1356.

Gao S., Rudnick R., Carlson R. W., McDonough W. F. and Liu Y.-S. (2002) Re–Os evidence for replacement of ancient mantle lithosphere beneath the North China craton. *Earth Planet. Sci. Lett.* **198**, 307–322.

Gérard O. and Jaoul O. (1989) Oxygen diffusion in San Carlos olivine. *J. Geophys. Res.* **94**, 4119–4128.

Griffin W. L., Zhang A., O'Reilly S. Y. and Ryan C. G. (1998) Phanerozoic evolution of the lithosphere beneath the Sino-Korean craton. In *Mantle Dynamics and Plate Interactions in East Asia*, vol. 27 (eds. M. F. J. Flower, S.-L. Chung, C.-H. Lo and T.-Y. Lee). AGU, Washington, DC, pp. 107–126.

Handler M. R., Baker J. A., Schiller M., Bennett V. C. and Yaxley G. M. (2009) Magnesium stable isotope composition of Earth's upper mantle. *Earth Planet. Sci. Lett.* **282**, 306–313.

Heimann A., Beard B. L. and Johnson C. M. (2008) The role of volatile exsolution and sub-solidus fluid/rock interactions in producing high ^{56}Fe/^{54}Fe ratios in siliceous igneous rocks. *Geochim. Cosmochim. Acta* **72**, 4379–4396.

Hoefs J. (1997) *Stable Isotope Geochemistry*, fourth ed. Springer-Verlag, Berlin, pp. 74–75.

Huang F., Lundstrom C. C., Glessner J., Ianno A., Boudreau A., Li J., Ferre E. C., Marshak S. and Defrates J. (2009a) Chemical and isotopic fractionation of wet andesite in a temperature gradient: experiments and models suggesting a new mechanism of magma differentiation. *Geochim. Cosmochim. Acta* **73**, 729–749.

Huang F., Glessner J., Ianno A., Lundstrom C. and Zhang Z. (2009b) Magnesium isotopic composition of igneous rock standards measured by MC-ICP-MS. *Chem. Geol.* **268**, 15–23.

Huang F., Chakraborty P., Lundstrom C. C., Holmden C., Glessner J. J. G., Kieffer S. and Lesher C. E. (2010a) Isotope fractionation in silicate melts by thermal diffusion. *Nature* **464**, 396–400.

Huang S.-C., Farkaš J. and Jacobsen S. B. (2010b) Calcium isotopic fractionation between clinopyroxene and orthopyroxene from mantle peridotites. *Earth Planet. Sci. Lett.* **292**, 337–344.

Ionov D. A., Chanefo I. and Bodinier J.-L. (2005) Origin of Fe-rich lherzolites and wehrlites from Tok, SE Siberia by reactive melt percolation in refractory mantle peridotites. *Contrib. Mineral. Petrol.* **150**, 335–353.

Jahn B. M., Auvray B., Cornichet J., Bai Y. L., Shen Q. H. and Liu D. Y. (1987) 3.5 Ga old amphibolites from eastern Hebei Province, China: field occurrence, petrography, Sm–Nd isochron age and REE geochemistry. *Precambrian Res.* **34**, 311–346.

Laan S. V. D., Zhang Y., Kennedy A. K. and Wyllie P. J. (1994) Comparison of element and isotope diffusion of K and Ca in multicomponent silicate melts. *Earth Planet. Sci. Lett.* **123**, 155–166.

Lesher C. E. (1990) Decoupling of chemical and isotopic exchange during magma mixing. *Nature* **344**, 235–237.

Lesher C. E. (1994) Kinetics of Sr and Nd exchange in silicate liquids theory, experiments, and applications to uphill diffusion, isotopic equilibration, and irreversible mixing of magmas. *J. Geophys. Res.* **99**(B5), 9585–9604.

Li S. G., Xiao Y. L., Liou D. L., Chen Y. Z., Ge N. J., Zhang Z. Q., Sun S. S., Cong B. L., Zhang R. Y., Hart S. R. and Wang S. S. (1993) Collision of the North China and Yangtse Blocks and formation of coesite-bearing eclogites – timing and processes. *Chem. Geol.* **109**, 89–111.

Li W.-Y., Teng F.-Z., Ke S., Rudnick R. L., Gao S., Wu F.-Y. and Chappell B. W. (2010) Heterogeneous magnesium isotopic composition of the upper continental crust. *Geochim. Cosmochim. Acta* **74**, 6867–6884.

Liu S.-A., Teng F.-Z., He Y.-S., Ke S. and Li S.-G. (2010) Investigation of magnesium isotope fractionation during granite differentiation: implication for Mg isotopic composition of the continental crust. *Earth Planet. Sci. Lett.* **297**, 646–654.

Lundstrom C. C., Marshak S., DeFrates J. and Mabon J. (2011) Alternative processes for developing fabric and mineral compositional zoning in intrusive rocks. *Int. Geol. Rev.* **53**, 377–405.

Mattey D., Lowry D. and Macpherson C. (1994) Oxygen isotope composition of mantle peridotite. *Earth Planet. Sci. Lett.* **128**, 231–241.

Menzies M. A. and Xu Y. (1998) Geodynamics of the North China Craton. In *Mantle Dynamics and Plate Interactions in East Asia*, vol. 27 (eds. M. F. J. Flower, S.-L. Chung, C.-H. Lo and T.-Y. Lee). AGU, Washington, DC.

Norman M. D., Yaxley G. M., Bennett V. C. and Brandon A. D. (2006) Magnesium isotopic composition of olivine from the Earth, Mars, Moon, and pallasite parent body. *Geophys. Res. Lett.* **33**, L15202. doi:10.1029/2006GL026446, 2006.

Pearson N. J., Griffin W. L. and O'Reilly S. Y. (2006) The isotopic composition of magnesium in mantle olivine: records of depletion and metasomatism. *Chem. Geol.* **226**, 115–133.

Poitrasson F. (2006) On the iron isotope homogeneity level of the continental crust. *Chem. Geol.* **235**, 195–200.

Poitrasson F. and Freydier R. (2005) Heavy iron isotope composition of granites determined by high resolution MC-ICP-MS. *Chem. Geol.* **222**, 132–147.

Poitrasson F., Halliday A. N., Lee D.-C., Levasseur S. and Teutsch N. (2004) Iron isotope differences between Earth, Moon, Mars and Vesta as possible records of contrasted accretion mechanisms. *Earth Planet. Sci. Lett.* **223**, 253–266.

Polyakov V. B. and Mineev S. D. (2000) The use of Mössbauer spectroscopy in stable isotope geochemistry. *Geochem. Geophys. Geosyst.* **64**, 849–865.

Putirka K. D. (2008) Thermometers and barometers for volcanic systems. *Rev. Mineral. Geochem.* **69**, 61–120.

Reisberg L., Zhi X., Lorand J.-P., Wagner C., Peng Z. and Zimmermann C. (2005) Re–Os and S systematics of spinel peridotite xenoliths from east central China: evidence for contrasting effects of melt percolation. *Earth Planet. Sci. Lett.* **239**, 286–308.

Richter F. M., Watson E. B., Mendybaev R., Teng F. Z. and Janney P. (2008) Magnesium isotope fractionation in silicate melts by chemical and thermal diffusion. *Geochim. Cosmochim. Acta* **72**, 206–220.

Richter F. M., Watson E. B., Mendybaev R., Dauphas N., Georg B., Watkins J. and Valley J. (2009) Isotopic fractionation of the major elements of molten basalt by chemical and thermal diffusion. *Geochim. Cosmochim. Acta* **73**, 4250–4263.

Schauble E. A. (2011) First-principles estimates of equilibrium magnesium isotope fractionation in silicate, oxide, carbonate and hexaaquamagnesium(2+) crystals. *Geochim. Cosmochim. Acta* **75**, 844–869.

Schoenberg R. and Blanckenburg F. V. (2006) Modes of planetary-scale Fe isotope fractionation. *Earth Planet. Sci. Lett.* **252**, 342–359.

Schoenberg R., Marks M. A. W., Schuessler J. A., Blanckenburg F. V. and Markl G. (2009) Fe isotope systematics of coexisting amphibole and pyroxene in the alkaline igneous rock suite of the Ilímaussaq Complex, South Greenland. *Chem. Geol.* **258**, 65–77.

Schuessler J. A., Schoenberg R. and Sigmarsson O. (2009) Iron and lithium isotope systematics of the Hekla volcano, Iceland – evidence for Fe isotope fractionation during magma differentiation. *Chem. Geol.* **258**, 78–91.

Teng F.-Z., Wadhwa M. and Helz R. T. (2007) Investigation of magnesium isotope fractionation during basalt differentiation: implications for a chondritic composition of the terrestrial mantle. *Earth Planet. Sci. Lett.* **261**, 84–92.

Teng F.-Z., Dauphas N. and Helz R. T. (2008) Iron isotope fractionation during magmatic differentiation in Kilauea Iki lava lake. *Science* **320**, 1620–1622.

Teng F.-Z., Li W.-Y., Ke S., Marty B., Dauphas N., Huang S., Wu F.-Y. and Pourmand A. (2010a) Magnesium isotopic composition of the Earth and chondrites. *Geochim. Cosmochim. Acta* **74**, 4150–4166.

Teng F.-Z., Li W.-Y., Rudnick R. L. and Gardner L. R. (2010b) Contrasting lithium and magnesium isotope fractionation during continental weathering. *Earth Planet. Sci. Lett.* **300**, 63–71.

Tipper E. T., Galy A. and Bickle M. J. (2006a) Riverine evidence for a fractionated reservoir of Ca and Mg on the continents: implications for the oceanic Ca cycle. *Earth Planet. Sci. Lett.* **247**, 267–279.

Tipper E. T., Galy A., Gaillardet J., Bickle M. J., Elderfield H. and Carder E. A. (2006b) The Mg isotope budget of the modern ocean: constraints from riverine Mg isotope ratios. *Earth Planet. Sci. Lett.* **250**, 241–253.

Tipper E. T., Louvat P., Capmas F., Galy A. and Gaillardet J. (2008a) Accuracy of stable Mg and Ca isotope data obtained by MC-ICP-MS using the standard addition method. *Chem. Geol.* **257**, 65–75.

Tipper E. T., Galy A. and Bickle M. J. (2008b) Calcium and magnesium isotope systematics in rivers draining the Himalaya–Tibetan-Plateau region: lithological or fractionation control? *Geochim. Cosmochim. Acta* **72**, 1057–1075.

Wombacher F., Eisenhauer A., Heuser A. and Weyer S. (2009) Separation of Mg, Ca and Fe from geological reference materials for stable isotope ratio analyses by MC-ICP-MS and double-spike TIMS. *J. Anal. At. Spectrom.* **24**, 627–636.

Weyer S., Anbar A. D., Brey G. P., Munker C., Mezger K. and Woodland A. B. (2005) Iron isotope fractionation during planetary differentiation. *Earth Planet. Sci. Lett.* **240**, 251–264.

Weyer S., Anbar A. D., Brey G. P., Münker C., Mezger K. and Woodland A. B. (2007) Fe-isotope fractionation during partial melting on Earth and the current view on the Fe-isotope budgets of the planets (reply to the comment of F. Poitrasson and to the comment of B.L. Beard and C.M. Johnson on "Iron isotope fractionation during planetary differentiation" by S. Weyer, A.D. Anbar, G.P. Brey, C. Münker, K. Mezger and A.B. Woodland). *Earth Planet. Sci. Lett.* **256**, 638–646.

Weyer S. and Ionov D. A. (2007) Partial melting and melt percolation in the mantle: the message from Fe isotopes. *Earth Planet. Sci. Lett.* **259**, 119–133.

Wiechert U. and Halliday A. N. (2007) Non-chondritic magnesium and the origins of the inner terrestrial planets. *Earth Planet. Sci. Lett.* **256**, 360–371.

Williams H. M., Mccammon C. A., Peslier A. H., Halliday A. N., Teutsch N., Levasseur S. and Burg J.-P. (2004) Iron isotope fractionation and the oxygen fugacity of the mantle. *Science* **304**, 1656–1659.

Williams H. M., Peslier A. H., Mccammon C., Halliday A. N., Levasseur S., Teutsch N. and Burg J.-P. (2005) Systematic iron isotope variations in mantle rocks and minerals: the effects of partial melting and oxygen fugacity. *Earth Planet. Sci. Lett.* **235**, 435–452.

Yang W., Teng F.-Z. and Zhang H.-F. (2009) Chondritic magnesium isotopic composition of the terrestrial mantle: a case study of peridotite xenoliths from the North China craton. *Earth Planet. Sci. Lett.* **288**, 475–482.

Young E. D., Galy A. and Nagahara H. (2002) Kinetic and equilibrium mass-dependent isotope fractionation laws in nature and their geochemical and cosmochemical significance. *Geochim. Cosmochim. Acta* **66**, 1095–1104.

Young E. D. and Galy A. (2004) The isotope geochemistry and cosmochemistry of magnesium. *Reviews in Mineralogy ; Geochemistry* **55**, 197–230.

Young E. D., Tonui E., Manning C. E., Schauble E. and Macris C. A. (2009) Spinel–olivine magnesium isotope thermometry in the mantle and implications for the Mg isotopic composition of Earth. *Earth Planet. Sci. Lett.* **288**, 524–533.

Zhang H.-F., Mattey D. P., Grassineau N., Lowry D., Brownless M., Gurney J. J. and Menzies M. A. (2000) Recent fluid processes in the Kaapvaal Craton, South Africa: coupled oxygen isotope and trace element disequilibrium in polymict peridotites. *Earth Planet. Sci. Lett.* **176**, 57–72.

Zhang S.-B., Zheng Y.-F., Wu Y.-B., Zhao Z.-F., Gao S. and Wu F.-Y. (2006) Zircon U–Pb age and Hf isotope evidence for 3.8 Ga crustal remnant and episodic reworking of Archean crust in South China. *Earth Planet. Sci. Lett.* **252**, 56–71.

Zhao X., Zhang H., Zhu X., Tang S. and Tang Y. (2010) Iron isotope variations in spinel peridotite xenoliths from North China Craton: implications for mantle metasomatism. *Contrib. Mineral. Petrol.* **160**, 1–14.

Zhu G., Wang Y., Liu G., Niu M., Xie C. and Li C. (2005) $^{40}Ar/^{39}Ar$ dating of strike-slip motion on the Tan-Lu fault zone, East China. *J. Struct. Geol.* **27**, 1379–1398.

Zhu X. K., Guo Y., Williams R. J. P., O'Nions R. K., Matthews A., Belshaw N. S., Canters G. W., Waal E. C. D., Weser U., Burgess B. K. and Salvato B. (2002) Mass fractionation processes of transition metal isotopes. *Earth Planet. Sci. Lett.* **200**, 47–62.

Associate editor: Alan D. Brandon